CHALMERS
UNIVERSITY OF TECHNOLOGY

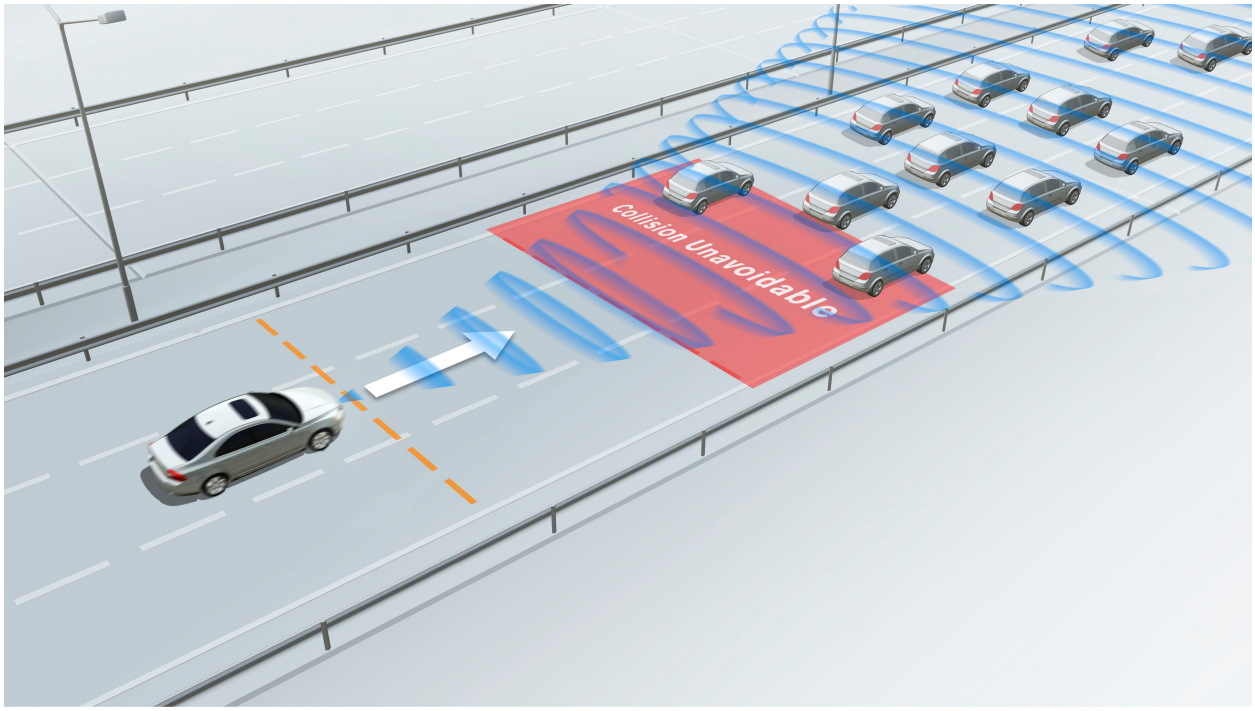

Combined Braking and Steering Maneuvers for Collision Avoidance

Master's thesis in Systems, Controls and Mechatronics

AXEL INGÓLFSSON, MITHILESH BHARDWAJ

Department of Electrical Engineering
CHALMERS UNIVERSITY OF TECHNOLOGY
Gothenburg, Sweden 2019

Master's thesis 2019

Analysis of potential benefits of combined braking and steering maneuvers over independent braking-and steering maneuvers for collision avoidance systems

AXEL INGÓLFSSON, MITHILESH BHARDWAJ

CHALMERS
UNIVERSITY OF TECHNOLOGY

Department of Electrical Engineering
Chalmers University of Technology
Gothenburg, Sweden 2019

Combined Braking and Steering Maneuvers for Collision Avoidance
AXEL INGÓLFSSON, MITHILESH BHARDWAJ

Supervisor: Gabriel Rodrigues de Campos (Zenuity AB) and Paolo Falcone (Chalmers Universisty of Technology)
Examiner: Paolo Falcone , Chalmers University of Technology

Master's Thesis 2019
Department of Electrical Engineering
Chalmers University of Technology
SE-412 96 Gothenburg
Telephone +46 31 772 1000

Cover: Combined Braking and Steering Maneuvers for Collision Avoidance

Typeset in LaTeX
Printed by Chalmers Reproservice
Gothenburg, Sweden 2019

Combined Braking and Steering Maneuvers for Collision Avoidance

AXEL INGÓLFSSON, MITHILESH BHARDWAJ
Department of Electrical Engineering
Chalmers University of Technology

Abstract

Nowadays, vehicles are equipped with advanced active safety systems, and in particular collision avoidance solutions that are designed to avoid traffic accidents by autonomously taking control of the vehicle in emergency situations. These systems include, for instance, AEB systems (Advanced Emergency Braking) that apply automatic braking in emergencies and eLKA systems (Emergency Lane Keeping Assist) that leverage steering actuation to drive the vehicle back to safety in lane departure situations.

In this thesis, we analyse the potential benefits of using combined braking and steering manoeuvres for collision avoidance. To perform this study, we have used two different approaches, i) reachability analysis and ii) simulation based analysis. For reachability analysis, a nonlinear mathematical model was derived and parameterized with realistic state and actuation constraint, and reachability computations were performed using the CORA (Continuous Reachability Analyzer) toolbox. A simulation based approach was also used to test and verify different combinations of steering and braking actuation in different traffic scenarios. Simulation results have shown that a system that leverages both braking and steering may be beneficial with respect to systems that use only one of these manoeuvres independently, in particular in cases involving stationary obstacles or pedestrians crossing the street.

Keywords: Modelling, simulation, reachability analysis, collision avoidance, active safety, AEB systems, eLKA systems.

Legal disclaimer:

In this thesis, the authors may refer to reference collision avoidance systems and simulation environments. Information presented concerns reference solutions and simulation environments under development, at a given point in time, and conclusions made based on such information shall be considered at that same point in time. Zenuity and the authors of this thesis are not responsible for the accuracy and performance of such information, nor the legal or other consequences of use or analysis of the information.

Acknowledgements

During our research, we were privileged enough to receive help and support from a number of people in the academia and at Zenuity whom we would like to take the opportunity to thank.
First of all we would like to express our gratitude to our supervisors, Paolo Falcone at Chalmers and Gabriel Rodrigues de Campos at Zenuity who dedicated an enormous amount of time and effort to assist us with our research. We would also like to thank Andrew Backhouse, Karthik Venkataraman and Mattias Brännström at Zenuity and Ankit Gupta at Chalmers for their constructive comments, suggestions and participation in brainstorming sessions. We are also grateful to the people at Zenuity for sharing their experience and knowledge with us and we would like to extend our special thanks to Caroline Stolt, Oscar Björk and Jenny Nilsson for their support with Zenuity's software and data. We would also like to acknowledge the team of CORA toolbox, in particular Dr. Mattias Althoff and Niklas Kochdumper who were very responsive to all of our questions and feature request.

AXEL INGÓLFSSON, MITHILESH BHARDWAJ, Gothenburg, March 2019

Contents

List of Figures

List of Tables

1

Introduction

1.1 Background

Nearly 1.3 million human lives are lost to road accidents every year worldwide and accidents are even the number one cause of death of young people between the ages of 15 and 29 [23]. However, with increasing road and vehicle's safety, these numbers have been decreasing all over the globe. For example, fatal road accidents in Sweden decreased by more then 45 % between 2007 and 2015 as reported in [22].

Automation's history goes back to 1930s, though it wasn't until late 1980s and early 1990s when state and private funded research programs were started in the United States, Europe and Japan to develop the idea of automated transportation systems [11]. Early vehicle safety research was focused on advanced highway systems with the objective to maximize highway capacity by automating highways and vehicles. These explorations needed measures both on infrastructure and on vehicle level. On the grounds of financial and practical limitations, there was shift from *Automated Highway Systems* (AHS) to *Intelligent Vehicle Initiative* (IVI) to accentuate driver assist systems as such could be implemented independently in different generation of cars without pricey modifications in the infrastructure.

Vehicle safety systems are often divided into two categories: i) passive safety, which aims at reducing the impact on occupants in case of a collision and ; ii) active safety which refers to safety features designed to prevent a collision in the first place. Active safety systems that predict approaching collisions based on the perception of the environment, and act accordingly by autonomously taking control of the vehicle are known as *Collision Avoidance* (CA) systems. CA systems leverage vehicle sensors to detect other traffic participants, and perform safe maneuvers to prevent or, worst case, mitigate accidents by adopting different decision controlling strategies.

The enormous success of AEB systems in traffic scenarios has long been proved. In 2012, EURO NCAP predicted that equipping all vehicles with AEB systems could result in a reduction of road accidents of 27 %, which could represent 8000 lives saved per year on European Roads [18]. The US Insurance Institute for Highway Safety

showed in a comparison that third party claims and personal injury claims from drivers of Volvo XC60 (2010 - 2012) and Volvo S60 (2011 - 2012) vehicles equipped with standard City AEB systems were 15 % and 26 % less common, respectively, than claims from a control group [18].

1.2 Purpose

The objective of this thesis is to examine the advantages of using a combination of steering and braking for collision avoidance, with respect to conventional systems that only leverage one of these maneuvers at a time. The results should be presented in a measurable way, such that their reliability can be validated.

1.3 Related Work

An important element of any CA system is an accurate threat assessment (TA). Numerous researches have been conducted on this topic. In [7], an extensive literature study about different TA techniques is given. At a macro level, the techniques can be divided into physical model based and data driven techniques. As the name suggests, the physical model based techniques are based on apprehension of the physical dynamics of the system while the data driven techniques are based on exploiting large amount of data and deriving comprehensive results from it. Physical model based techniques are further subdivided into single-behavior threat metrics (SBTMs), optimization-based methods, formal methods and probabilistic approaches. Different metrics like system performance, real time properties, robustness, etc, were adopted to establish advantages and disadvantages of different methods. For example, probabilistic methods can use the complete range of uncertainty to compute probability of a collision so to improve performance, though are generally computationally expensive for a real time system. On the contrary, SBTMs are computationally efficient as they only consider the most likely state estimates, but that could hinder the system's performance and need empirical tuning .

Paden et al. [16] proposes a literature review on planning and control algorithms for self driving vehicles for urban setting. It also provides a hierarchy for decision making algorithms, where top-most layer commence with route planning using road network, which is followed by behavioral layer focusing on advancing the car to desired destination abiding to road regulations. The behavioral layer is then succeeded by motion planning to check for constraints, followed by feedback controller to minimize errors. Different motion models and motion planning methods have been considered, and their performance and computational requirements have been evaluated, which could be beneficial for accessing compatibility and computational trade-offs while performing system level design.

In [21], a tight over-approximation of reachable sets have been presented and is used to calculate Time-To-React (TTR) for risk assessment. Söentges et al. have used a speed and acceleration bounded point mass model to calculate the sets using the SPOT toolbox [13]. Reachable sets calculation is computationally efficient for the defined model and the approach is deterministic and consider uncertainties of other traffic participants.

Brännström et al. have proposed in [5] an algorithm for collision avoidance with other traffic participants by either steering, braking or accelerating. It is a model based approach, adopting a linear bicycle model and drivers' preferred parameters, which were obtained from a data set of 125 driving hours in real traffic by a mixture of drivers spanning a total distance of almost 8000 km. One of the main advantages of the proposed algorithm is that it can be used for any vehicle (cycles, cars, trucks) and is valid for various traffic scenarios. Furthermore, the results indicate that it improves the timing of autonomous brake activation for rear-end collision with respect to conventional threat assessment algorithms. Intervention timing of the proposed algorithm is shown in Figure 1.1.

In [10], robustness and computation complexity issues were discussed for a lane departure detection system. An MPC controller was used to recursively compute the vehicle's future trajectories based on its state and surroundings information. Semi-autonomous driving interventions with steering input were based on reachability analysis of this expected trajectory.

In [20], Shim et al. looked into simultaneous braking and steering actions for emergency driving support, using a *Nonlinear Model Predictive Controller* (NMPC). They compared their simulation results with a *Velocity Ratio Controller* (VRC) as a benchmark controller.

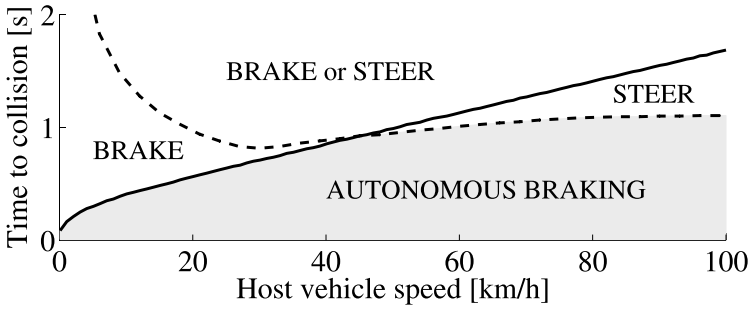

Figure 1.1: Illustration depicting when driver can avoid a collision by either only braking (solid) or only steering (dashed). Shaded region depicts when Autonomous braking is initiated. This figure is taken from [5], and is a courtesy of Mattias Brännström. All rights reserved.

Eckert et al. in [8] have shown the effect of TTCs and overlaps on the choice of emergency maneuver performed by a driver. The behavioral study was conducted on the Continental proving grounds in Frankfurt, Germany, where 41 drivers drove on a test track and were subjected to real life emergency situations. In addition to 100 % and 50 % overlaps, three different TTCs i.e, 1.5 s, 2 s and 2.5 s were considered for this track test. Moreover, another similar examination was performed on IOWA Driving Simulator, where speed limit was the second variable in addition to the variable TTCs. The results were consistent for the two examinations and yielded similar driving behavior. It was observed that drivers preferred braking only for longer TTCs, while steering activities increased as the TTC reduced.

In [2], M. Althoff performs in his PhD thesis an extensive research on how *zonotopes* can be used to represent and compute reachable sets of linear, non-linear and hybrid systems with a high number of states. Zonotopes are centrally symmetric polytopes that can be represented with much less data than conventional polytopes. Operations can be performed on so called generators instead of half spaces or vertices which allows fundamental operations for reachability analysis, such as *Minkowski addition* and *linear mapping*, to scale well with an increasing number of states. The centrally symmetrical nature of zonotopes is also one of their limiting factor, whereas operations such as calculating the convex hull or the intersection of two zonotopes do not necessarily yield centrally symmetrical objects, i.e. zonotopes. However, the convex hull can be tightly overapproximated and the intersection can be represented with either zonotope bundles, which M. Althoff introduced in [4], or with constrained zonotopes, which were introduced by J.K. Scott et al. in [19].

1.4 Structure of Report

Chapter 2 covers the comparison of different conventional vehicle models with the reference simulation environment, and the necessity of deriving a new model for combined braking and steering maneuvers. In Chapter 3 simulation results derived from RSE for various day to day traffic scenarios are presented. Chapter 4 focuses on the theory and methods used to perform reachability analysis in this thesis and also includes the results obtained from it. Conclusions and some suggestions for future work are presented in Chapter 5.

2

Modelling

In this chapter, we provide a mathematical model that transfers a steering input and a braking input into the vehicle states such as velocity and lateral- and longitudinal positions. Results are compared with the performance of standard vehicle models and with a Reference Simulation Environment (RSE).

2.1 Vehicle Models

There are many mathematical models in the literature describing vehicle dynamics. Existing models differ in e.g., their described vehicle dynamics and the balance between accuracy and simplicity. The practicality of each model also depends on the intended application. For instance, to perform formal analysis, such as reachability analysis, a Linear Time Invariant (LTI) model would be user friendly and convenient. However, such model entails several simplifications and approximations. In order to achieve reliable and precise results, a nonlinear model is necessary. In this section we introduce a brief introduction of two commonly used vehicle models that describe the lateral dynamics of a vehicle, and how they were used within this thesis work.

2.1.1 Kinematic Bicycle Model

The *kinematic bicycle model* is a simple nonlinear model that describes the lateral dynamics of a vehicle, transferring a pinion angle input into heading and lateral- and longitudinal positions. The model also depends on the vehicle's velocity, either as a parameter, or as a state variable, in which case the velocity is transferred from another input variable, the longitudinal acceleration. The name is derived from the abstraction where the left and the right wheels are lumped together into two wheels as in a bicycle, one in the front and one in the rear. Slip angles, which are the angles between the velocity vector of the vehicle and the wheels, are neglected along with all pitch and roll dynamics, leaving only simple yaw dynamics at the table. The kinematic bicycle model performs well in cases where a vehicle is travelling at a low speed [17]. However, when the vehicle exceeds a velocity of $5\,\mathrm{m\,s^{-1}}$, the assumption of the slip angle being negligible does not hold anymore. The kinematic bicycle model is shown in equation (2.1),

$$\begin{aligned} \dot{p}_x &= v \cdot \cos(\varphi), \\ \dot{p}_y &= v \cdot \sin(\varphi), \\ \dot{\varphi} &= \frac{v}{L} \tan(\delta), \\ \dot{v} &= a_{long}, \end{aligned} \tag{2.1}$$

where p_x and p_y are the longitudinal- and lateral positions, respectively, with respect to an initial inertial frame, v the vehicle's velocity, L the distance between the front and the rear wheels and φ the vehicle's heading. Moreover, δ and a_{long} are the input signals and denote the pinion angle and the vehicle's longitudinal acceleration, respectively.

2.1.2 Dynamic Bicycle Model

Another commonly used model is the *dynamic bicycle model*. As the name indicates, this model shares with the kinematic bicycle model the abstraction of combining the right and the left wheels into one front wheel and one rear wheel. Unlike the kinematic bicycle model, however, this model describes lateral dynamics of the vehicle with linear equations assuming that the velocity is kept constant. The dynamic bicycle model does not neglect slip angles. Instead, the slip angles of the wheels are used to approximate lateral forces on the wheels, which are then used to estimate the lateral velocity of the vehicle (denoted by $\dot{y}$) with respect to the vehicle's frame. The lateral forces are approximated as a term proportional to the slip angles, as shown in equation (2.2):

$$F_{yf} = 2C_{af}(\delta - \theta_{vf}), \tag{2.2}$$

where $2C_{af}$ represents the cornering stiffness of the front wheels, δ the wheel angle and θ_{vf} the slip angle. One can refer to [17] for further details. The dynamic bicycle model is described in equation (2.3),

$$\dot{\chi} = \begin{bmatrix} \frac{-2C_{af} + 2C_{ar}}{mv} & -v - \frac{2C_{af}l_f - 2C_{ar}l_r}{mv} \\ -\frac{2C_{af}l_f - 2C_{ar}l_r}{I_z v} & \frac{2C_{af}{l_f}^2 - 2C_{ar}{l_r}^2}{I_z} \end{bmatrix} \chi + \begin{bmatrix} \frac{2C_{af}}{m} \\ \frac{2l_f C_{af}}{I_z} \end{bmatrix} u, \tag{2.3}$$

where $\chi = \begin{bmatrix} \dot{y} & \dot{\varphi} \end{bmatrix}^T$, $u = \delta$ and the remaining parameters are defined as follows,

l_f : Distance between the front wheels and the vehicle's center of gravity.
l_r : Distance between the rear wheels and the vehicle's center of gravity.
m : Vehicle's mass.
v : Vehicle's velocity.
I_z : Vehicle's inertia around the yaw axis.
C_{af} : Cornering stiffness at front wheel.
C_{ar} : Cornering stiffness at rear wheel.

Note that the inertia I_z and the cornering stiffnesses C_{ar} and C_{af} vary with velocity and can therefore only be considered constant if the velocity v is constant.

By default, the dynamic bicycle model does not track longitudinal- or lateral- positions of the vehicle with respect to an inertial frame. Only two state variables are tracked: the yaw rate $\dot{\varphi}$ and the lateral velocity with respect to the body frame, $\dot{y}$. With modifications, the heading can be observed by integrating the yaw rate over time and the lateral position can be tracked by integrating the lateral velocity with respect to the inertial frame using:

$$\dot{\varphi} = v \cdot \sin(\varphi).$$

Note that the state variable $\dot{y}$ denotes the lateral velocity with respect to the vehicle frame, not the inertial frame. Therefore, integrating $\dot{y}$ does not yield the lateral position of the vehicle. Using a *small angle approximation*, which entails on approximating ($\sin\varphi \approx \varphi$) when φ is small, the following equation holds.

$$\dot{\chi} = \begin{bmatrix} 0 & 0 & v & 0 \\ 0 & \dfrac{-2C_{af}+2C_{ar}}{mv} & 0 & -v - \dfrac{2C_{af}l_f - 2C_{ar}l_r}{mv} \\ 0 & 0 & 0 & 1 \\ 0 & -\dfrac{2C_{af}l_f - 2C_{ar}l_r}{I_z v} & 0 & \dfrac{2C_{af}{l_f}^2 - 2C_{ar}{l_r}^2}{I_z v} \end{bmatrix} \chi + \begin{bmatrix} 0 \\ \dfrac{2C_{af}}{m} \\ 0 \\ \dfrac{2l_f C_{af}}{I_z} \end{bmatrix} u \qquad (2.4)$$

where $\chi = \begin{bmatrix} p_y & \dot{y} & \varphi & \dot{\varphi} \end{bmatrix}^T$ and $u = \delta$.

Furthermore, by using longitudinal acceleration as an input, velocity can also be termed as a state variable instead of a parameter. This would however result in a nonlinear model, and the cornering stiffness constants and the vehicle's inertia around the yaw axis can at best act as approximations when the vehicle is not driving at the velocity these constants were derived for. The augmented dynamic bicycle model for varying velocity is shown in equation (2.5):

$$
\begin{aligned}
\dot{p}_x &= v \cdot \cos\varphi, \\
\dot{p}_y &= v \cdot \sin\varphi, \\
\dot{v} &= u_1, \\
\dot{y} &= \dot{y}, \\
\ddot{y} &= \frac{2}{mv}\left(C_{af} - C_{ar}\right)\dot{y} - v - \frac{2}{mv}\left(C_{af}l_f - C_{ar}l_r\right)\dot{\varphi} + \frac{2C_{af}}{m}u_2, \\
\ddot{\varphi} &= \frac{2}{I_z v}\left(C_{af}l_f - C_{ar}l_r\right)\dot{y} + \frac{2}{I_z v}\left(C_{af}l_f^2 - C_{ar}l_r^2\right)\dot{\varphi} + \frac{2l_f C_{af}}{I_z}u_2,
\end{aligned}
\tag{2.5}
$$

where u_1 represents the longitudinal acceleration and u_2 the pinion angle.

2.2 Reference simulation environment

The main platform used to run tests,‘ collect data and benchmark our results against is the Reference Simulation Environment (RSE). RSE, is a realistic simulation environment, with a four wheel vehicle modelling incorporated with sensor and actuation modelling, which enabled us to run a series of simulations to analyze the vehicle's response to different combinations of steering and braking inputs. RSE logs a number useful state parameters such as lateral- and longitudinal- velocity, lateral- and longitudinal- acceleration, real-time information about lane markers, other vehicles on the road, etc. Some important state parameters that are either time dependant or relative to an inertial frame are not logged by RSE but can be observed from other parameters. For example, the lateral position and the heading of the vehicle can be tracked by comparing the position and angles of the road markers to an initial position and angle of the road markers. The longitudinal position can be tracked by integrating the velocity over time.

The vehicle model in the RSE has two inputs: deceleration request in $[\mathrm{m\,s^{-2}}]$ and; steering angle request, i.e., the requested angle of the steering wheel in [rad]. Multiplying the pinion angle with the *steering ratio*, which is the ratio between the wheel steering angle and the *pinion angle*, yields the *steering wheel angle*. The pinion angle is the angle between the front wheels and the vehicles's heading. There are naturally dynamics between the requested and the actual deceleration and steering angle. Minor dynamics can in some cases be described with delays and saturations, but heavier dynamics may need additional integrators to be described accurately enough.

Figure 2.1 shows how the RSE responds to a constant deceleration request in Figure 2.1a and a constant steering angle request in Figure 2.1b. One can see that there is a delay of a few hundred milliseconds between the requested deceleration and the system's response due to pressure build up in the braking system, but the response is overall accurate. The dynamics between the requested steering angle and the pinion angle response are not as simple whereas the system response corresponds to a second order like system.

One may also notice that the pinion angle saturates at a much lower angle than the requested 1°. This is due to a torque limit in the steering actuator which affects both the angular acceleration of the steering wheel and the angular velocity, although the angular velocity can be neglected due to a low friction in the steering wheel. The maximum steering wheel angle is also affected since a large pinion angle results in a large yaw rate of the vehicle and therefore a large lateral counter-force from the tires. This counter-force is also affected by the velocity of the vehicle. Hence the following holds:

$$\left|\tau(\delta, v) + c\ddot{\delta}\right| \leq \tau_{max}, \tag{2.6}$$

where $\tau(\delta, v)$ is the torque needed to keep the pinion angle at δ radians, at velocity v, $\ddot{\delta}$ is the angular acceleration of the steering wheel, τ_{max} the maximum torque available to turn the steering wheel and c is a constant.

2.2.1 Comparison between mathematical models and simulations with RSE

In order to show the accuracy of the dynamic- and the kinematic-bicycle models, the RSE was used to obtain a vehicle trajectory, and the state responses were compared to the state responses obtained with the two different bicycle models. In Figure 2.2, simulation results are shown for a vehicle at an initial velocity of $70\,\mathrm{km\,h^{-1}}$, for which a constant deceleration signal of $12\,\mathrm{m\,s^{-2}}$ is requested along with a steering angle that corresponds to a pinion angle of 2.5°. In the left figure the RSE's pinion angle and the forward acceleration responses are shown, while the right figure shows the lateral acceleration and lateral position responses, along with the corresponding state responses from the kinematic- and the dynamic bicycle models. Note that the difference between Figure 2.1 and Figure 2.2 is that former shows two graphs where braking and steering has been requested separately and the latter where a

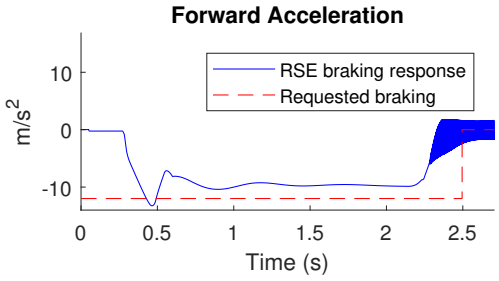

(a) Deceleration response of RSE when a deceleration of $12\,\mathrm{m\,s^{-2}}$ is requested. Note that there is a delay of a few hundred milliseconds due to the pressure build-up. The deceleration response saturates at around 1 g.

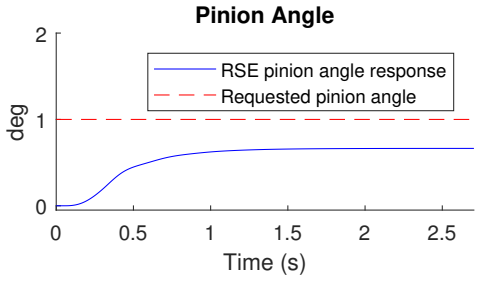

(b) Pinion angle response of RSE when a pinion angle of 1° is requested.

Figure 2.1: RSE pinion angle and deceleration response to constant inputs, for a vehicle speed of $70\,\mathrm{km\,h^{-1}}$.

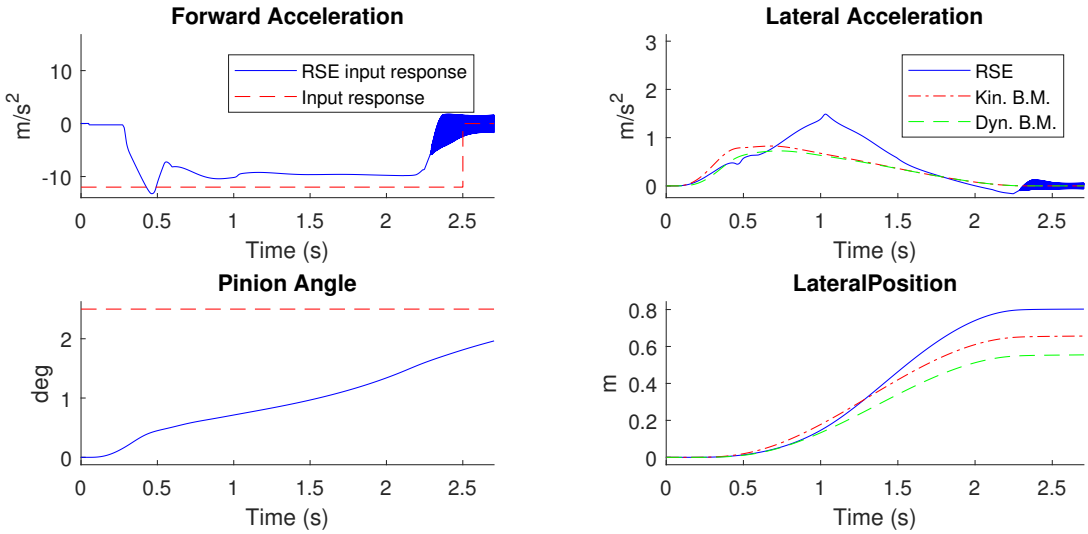

(a) Forward acceleration and pinion angle response from RSE.

(b) Lateral acceleration and lateral position responses of the kinematic- and dynamic bicycle models and RSE.

Figure 2.2: Comparison between RSE and the kinematic- and dynamic bicycle models when requesting a constant deceleration of $12\,\mathrm{m\,s^{-1}}$ and a constant pinion angle of 2.5° for an initial velocity of $70\,\mathrm{km\,h^{-1}}$.

combination of braking and steering has been requested simultaneously. The bicycle models were fed with the input responses in Figure 2.2a.

When steering and braking are applied simultaneously, the kinematic and the dynamic bicycle models significantly under-approximate the lateral acceleration and therefore the lateral position reached by the vehicle. This happens because the pitch level, caused by the vehicle's rapid deceleration, leads to a weight transfer from the rear to the front wheels which results in an higher yaw rate than predicted. The body pitch and the normal tire forces are shown in Figure 2.3.

From these simulation results it is clear that the kinematic- and the dynamic bicycle models, that take yaw dynamics into account but reject pitch and roll dynamics, fall short in predicting the lateral states of a vehicle when exposed to steering and braking requests at the same time.

2.3 Modelling: Dynamics and Constraints

As previously shown in Figure 2.1, the dynamics behind the braking and the steering actuators are cannot be neglected and must therefore be modelled to a suitable extent. These dynamics are however quite independent from the rest of the vehicle dynamics as they do not significantly affect each other, and were therefore modelled separately in the context of this work. A diagram of the decoupled dynamics of the

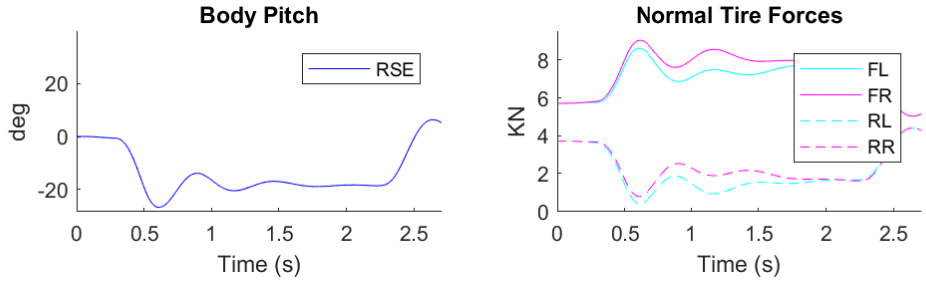

Figure 2.3: The left figure shows the body pitch of the vehicle when a deceleration of $1\,\mathrm{m\,s^{-2}}$ is requested from an initial velocity of $70\,\mathrm{km\,h^{-1}}$ along with a pinion angle of 1°. The right figure are the normal tire forces. The solid lines denote the front tires and the dashed lines the rear tires. The tires on the left side are denoted with a cyan color and the tires on the right side with magenta color. When the vehicle's brakes are applied rapidly, the vehicle is exposed to a significant body pitch which results in a weight transfer from the rear wheels to the front wheels.

system is shown in Figure 2.4.

2.3.1 Vehicle dynamics

In order to analyze how the maximum steering angle that can be obtained is related to other state variables, a number of simulations were ran where a high steering angle was requested while the brakes were being applied. This experiment was repeated with a range of deceleration values, ranging between $0.3\,\mathrm{g}$ and $1\,\mathrm{g}$, where g is maximum deceleration of the vehicle corresponding to $9.82\,\mathrm{m\,s^{-2}}$, and for initial velocities ranging between $50\,\mathrm{km\,h^{-1}}$ and $130\,\mathrm{km\,h^{-1}}$.

Figure 2.5 shows the relationship between lateral acceleration and velocity obtained from the simulations performed. One can observe that for lower velocities, the vehicle's lateral acceleration and velocity are constrained with an affine relationship given as:

$$|a_{lat}| \leq c_1 v + c_2, \tag{2.7}$$

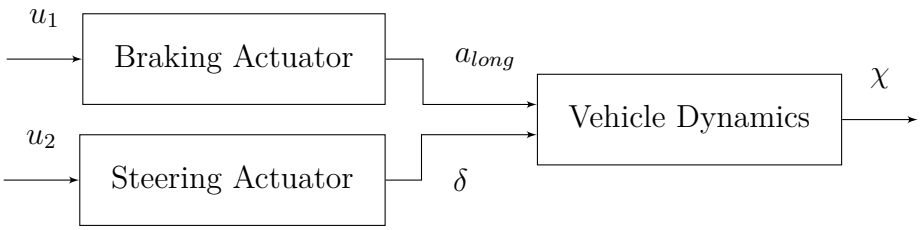

Figure 2.4: Illustration of the system architecture. In this thesis, the braking and the steering actuators were modelled separately. u_1 and u_2 are the inputs to the braking- and the steering actuators, respectively, a_{long} is longitudinal acceleration, δ is the pinion angle and x are the vehicle states.

where c_1 and c_2 are constants, v is velocity and a_{lat} is lateral acceleration. The affine constraints in (2.7) have been highlighted with a black dashed line.

Additionally , in order to cope with comfort limitations of the maneuvers, the lateral acceleration has been upper bounded to $2.5\,\mathrm{m\,s^{-2}}$. Note that, by taking the box constraints into account, the area between the black dashed line and the gray dashed line is the potential lateral acceleration that is compromised by approximating the constraints between lateral acceleration and velocity with the affine relationship.

With respect to the bicycle models given in equations (2.1) and (2.5), which are controlled by the pinion angle, the constraints can be formulated as a nonlinear constraint given as:

$$\delta = \arctan\left(L \cdot \frac{a_{lat}}{v^2}\right) \tag{2.8}$$

where L is the length between the front and the rear tires of the vehicle.

By leveraging equation (2.8), one could bypass the dynamics between the pinion angle and the heading of the vehicle and control the system directly by lateral acceleration instead. If the potential lateral acceleration of the vehicle can be predicted

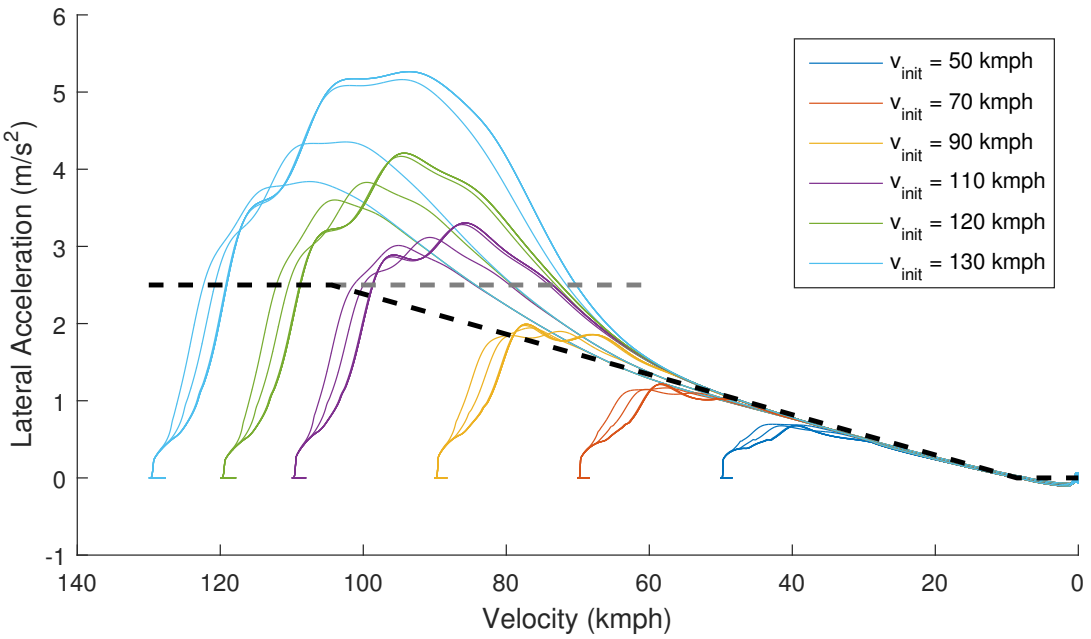

Figure 2.5: This figure shows the relationship between lateral acceleration and velocity obtained from a number of simulations where braking and steering was applied at the same time. The steering angle request signal was kept high in order ensure that the lateral acceleration would always be maximized. The colors indicate different initial velocities from which the maneuvers were applied and the different responses shown for each color indicate different values of requested deceleration. For lower velocities, the lateral acceleration does not exceed an affine function of the velocity of the vehicle. This relationship between lateral acceleration and velocity is highlighted with a black dashed line. A maximum lateral acceleration constraint of $2.5\,\mathrm{m\,s^{-2}}$ is indicated with a dashed line.

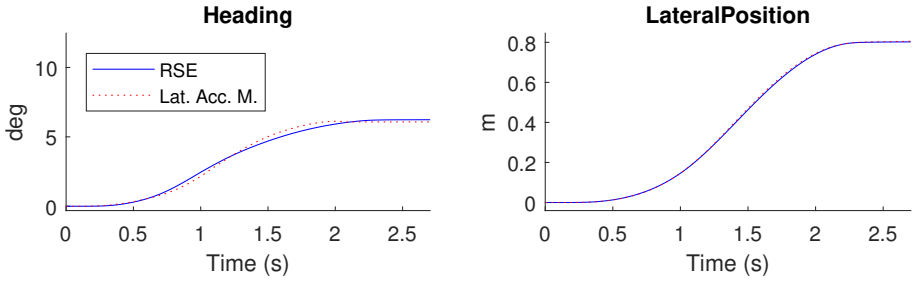

Figure 2.6: The heading and lateral position response of the model demonstrated with equation (2.9) when fed with longitudinal- and lateral acceleration response from RSE, shown in figure 2.2b. The states are predicted with significantly more accuracy using this model than with the bicycle models (figure 2.2a). The lateral position curves are almost identical and can hardly be distinguished from one another.

accurately enough by the affine constraints, then the heading and eventually the lateral- and longitudinal positions can also be predicted with significantly more accuracy.

Note that $c_2 > 0$ in (2.7), and therefore it prevents the velocity from going below a certain value $v = -\frac{c_2}{c_1}$. To work around this issue, the yaw rate is set to zero for velocities lower than this value. This should not affect the final results significantly in terms of lateral- and longitudinal positions, since the vehicle is not moving a lot at velocities this low anyway. A model that transfers lateral- and longitudinal acceleration into velocity, heading and lateral- and longitudinal positions is given in the following:

$$\begin{aligned} \dot{p}_x &= v \cdot \cos\varphi \\ \dot{p}_y &= v \cdot \sin\varphi \\ \dot{\varphi} &= \begin{cases} \dfrac{a_{lat}}{v}, & v \geq -\dfrac{c_2}{c_1} \\ 0, & v < -\dfrac{c_2}{c_1} \end{cases} \\ \dot{v} &= a_{long} \end{aligned} \tag{2.9}$$

Passing the lateral acceleration response from RSE, shown in Figure 2.2a, into a model demonstrated in equation (2.9), yields the heading and the lateral position response shown in Figure 2.6. The response shown in this figure is significantly closer to the response obtained with RSE when compared to the response from the bicycle models in Figure 2.2b.

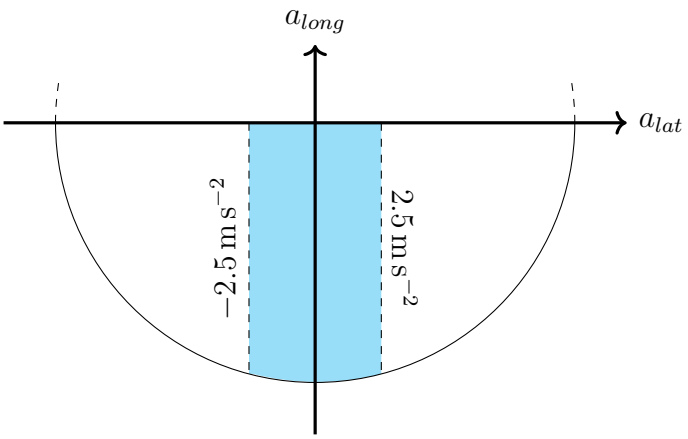

Figure 2.7: The half-circular curve is a GG-diagram of a vehicle. A GG-diagram demonstrates the physical limitation of how the total acceleration of a vehicle can be distributed between lateral- and longitudinal acceleration. For the application of this thesis, the vehicle shouldn't exceed a lateral acceleration of $2.5\,\mathrm{m\,s^{-2}}$ which yields blue area as the area of interest.

2.3.2 GG-Constraints

For the sake of completeness of the model, one should also consider that maximum acceleration a vehicle can physically handle, for the most part due to friction on the tires. Diagrams that demonstrate how the net acceleration of a vehicle can be distributed between longitudinal- and lateral acceleration are known as *GG-diagrams*. GG-diagrams show that maximum deceleration can only be achieved when no steering is applied and the more lateral acceleration is requested, the more braking power needs to be compromised. The bottom half of a GG-diagram, that is the part that accounts for steering and braking but not positive longitudinal acceleration, is shown in Figure 2.7.

The blue area in the figure is the area where the maximum lateral acceleration constraints and the constraints from the GG-diagram are fulfilled, and where the model should operate.

2.3.3 Input actuation dynamics

The dynamics of the braking and the steering actuators can be roughly described with simple models. The braking actuator i.e., the transfer from the first input u_1 to longitudinal acceleration, is approximated with an input delayed first order system, while the second input u_2 is approximated with an input delayed second order system. The full model, including the input actuators, is given as:

$$\dot{p}_x = v \cdot \cos\varphi \tag{2.10a}$$
$$\dot{p}_y = v \cdot \sin\varphi \tag{2.10b}$$
$$\dot{\varphi} = \begin{cases} \frac{a_{lat}}{v}, & v \geq -\frac{c_2}{c_1} \\ 0, & v < -\frac{c_2}{c_1} \end{cases} \tag{2.10c}$$
$$\dot{v} = u_1(t - \tau_1) \tag{2.10d}$$
$$\dot{a}_{lat} = j_{lat} \tag{2.10e}$$
$$\dot{j}_{lat} = u_2(t - \tau_2) \tag{2.10f}$$
$$\tag{2.10g}$$

subject to the constraints:

$$|a_{lat}| - c_1 \cdot v \leq c_2 \tag{2.11a}$$
$$|a_{lat}| \leq 2.5\,\mathrm{m\,s^{-2}} \tag{2.11b}$$
$$v \geq 0 \tag{2.11c}$$
$$a_{lat}^2 + a_{long}^2 \leq a_{max}^2 \tag{2.11d}$$
$$a_{long} \in [-a_{max}, 0] \tag{2.11e}$$

Validating the reliability of these input actuators with RSE simulations is not straight-forward. The steering actuator predicts the lateral acceleration of the vehicle through a double integrator while the RSE vehicle is controlled with a steering angle request. It has already been shown that when the vehicle's brakes are applied, the relationship between velocity, lateral acceleration and pinion angle in equation (2.8) does not hold. In order to work around this problem the pinion angle request was regulated with a PID controller, as demonstrated in Figure 2.8.

Note that a PID introduces rising time and it definitely does not guarantee the full potential of the RSE vehicle to be delivered. However, this can be used to verify that the input actuator is at least conservative.

The full model including all constraints, defined in equation (2.10), was simulated with a combined braking and steering maneuver, where a maximum lateral input was requested and the maximum deceleration signal that could be afforded with respect to the GG-diagram, given the lateral acceleration at each time step. The simulation was repeated from three different initial velocities and are shown in Figure 2.9 for $70\,\mathrm{km\,h^{-1}}$, Figure 2.10 for $90\,\mathrm{km\,h^{-1}}$ and Figure 2.11 for $120\,\mathrm{km\,h^{-1}}$. The lateral acceleration graph shows the performance of the steering actuator and the velocity shows the performance of the braking actuator.

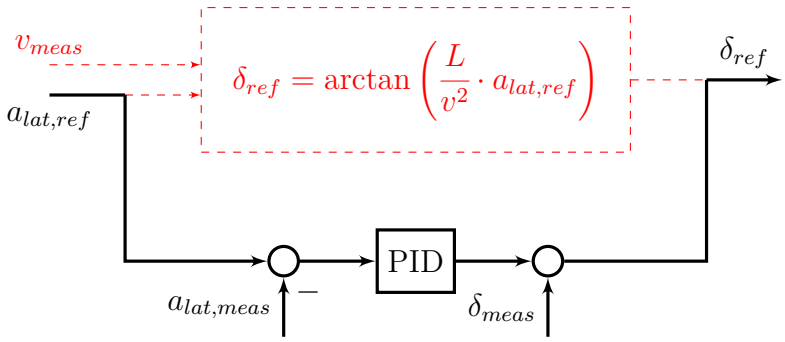

Figure 2.8: The vehicle in RSE is controlled with a steering angle request. When the vehicle is driving at a constant velocity, a steering angle needed to obtain a certain lateral acceleration can be calculated with equation (2.8). However, when the brakes are applied, this relationship does not anymore due to weight transfer from the rear wheels to the front wheels. Therefore, instead of using equation (2.8), the steering angle request is regulated with a PID controller.

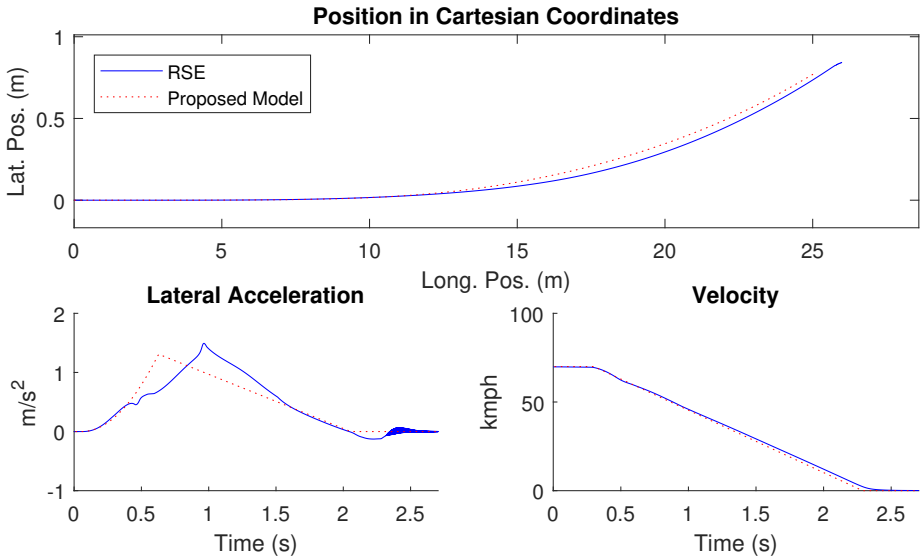

Figure 2.9: This figure shows how the mathematical model represented with equation (2.10) performs in comparison to RSE when steering and braking simultaneously from an initial velocity of $70\,\mathrm{km\,h^{-1}}$. The double integrator manages to build up lateral acceleration slightly faster than RSE, but when RSE catches up, the conservative constraints under-approximate how much lateral acceleration can be afforded. Due to the under-approximated lateral acceleration in the model, the longitudinal deceleration is reduced slightly in the model to make sure that constraints set by the GG-diagram are never violated.

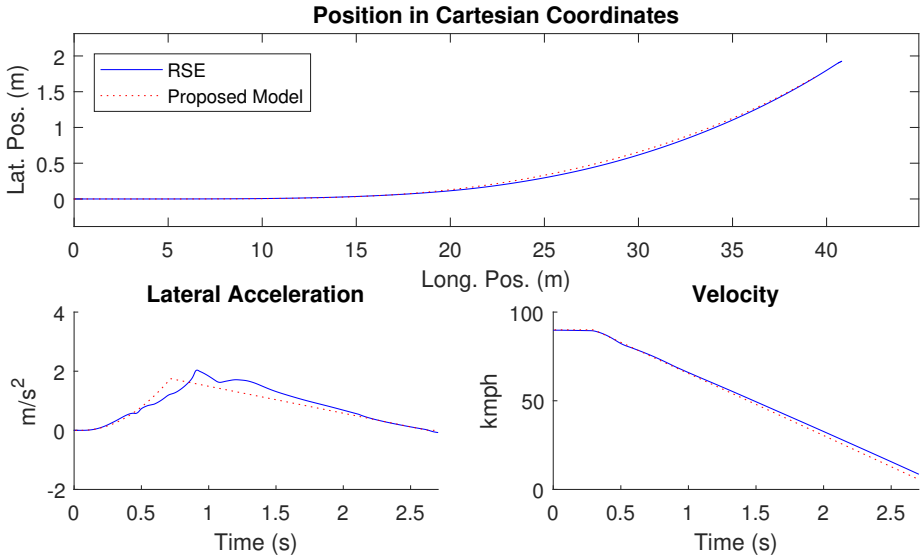

Figure 2.10: Braking and steering from an initial velocity of $90\,\mathrm{km\,h^{-1}}$. With a higher initial velocity, RSE manages to build up lateral acceleration faster and proportionally, and lateral acceleration overshoot is proportionally lower than in Figure 2.9. The resulting trajectory is more accurate.

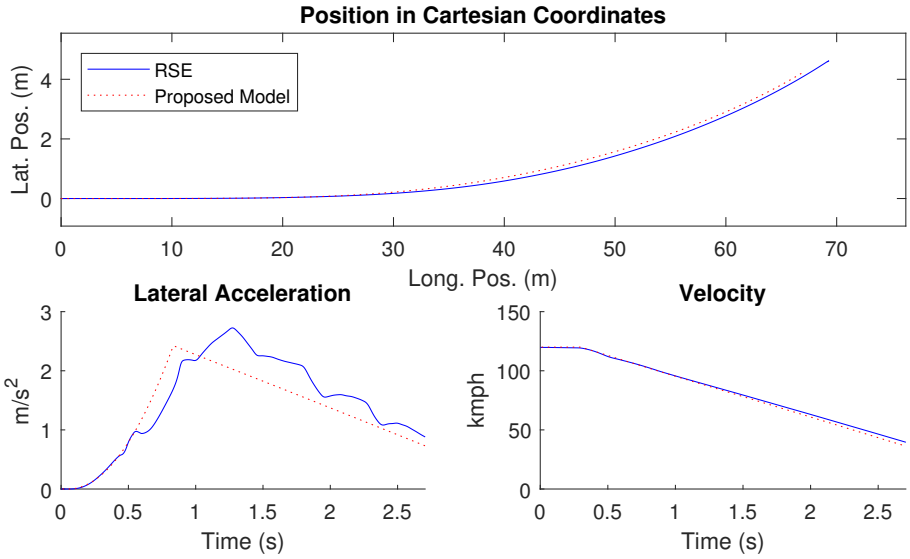

Figure 2.11: Braking and steering from an initial velocity of $120\,\mathrm{km\,h^{-1}}$. In this case the PID controller is struggling more with regulating the lateral acceleration.

3

Simulation Analysis

In this chapter we analyze the performance of a combined evasive maneuver of steering and braking for emergency traffic scenarios using a simulation based method. A number of simulations were performed using a reference simulation environment (RSE) where different combinations of steering and braking were applied and the performance of a combined braking and steering maneuver was compared to the performance of systems that leverage braking and steering separately. The comparisons made in this thesis are against reference collision avoidance systems that imitate the functionality of systems such as AEB- and eLKA systems, but do not represent actual production systems. The performance of different maneuvers are primarily measured in *TTR - Time To React*, which is defined as the latest *TTC - Time To Collision* at which an intervention able to avoid a collision can be triggered. One benefit of a simulation based approach over formal methods is that system complexities such as non-linearities, system constraints and complicated traffic scenarios can easily be simulated with a proper simulation environment, which minimizes the need for conservative system approximations.

However, this approach comes with the following drawbacks:

- It is not obvious how to optimally compromise between steering and braking in a combined maneuver in order to minimize TTR. Moreover, this combination can vary between different traffic scenarios. This may lead to an underestimation of performance of the maneuver.

- Simulations with the RSE are very slow which makes it infeasible to sweep for many variables between simulations, especially if the variables are densely sampled. The complexity grows exponentially with the number of variables and linearily with an increasing sampling resolution of each variable.

Finally, the obtained results will be used to demonstrate how a combined maneuver of steering and braking performs in different common traffic scenarios, including some Euro NCAP scenarios.

3.1 Approach description

Although it is not obvious how to optimally compromise between steering and braking in a combined maneuver as previously stated, some combinations can certainly be ruled out. For example, a combined maneuver cannot cause the host vehicle to decelerate down to a safe velocity faster than a pure braking maneuver can do. In Chapter 2, this was demonstrated with a GG-diagram in Figure 2.7 where it was shown that a lateral acceleration cannot be obtained without compromising how much longitudinal acceleration can be afforded simultaneously. The objective with a combined maneuver is therefore to reach a safe region by moving the host vehicle laterally along a trajectory that is safer than what can be achieved with a maneuver that only leverages steering.

One may also think of an optimal maneuver consisting of maximum braking and maximum steering requested simultaneously until the vehicle reaches a stationary position. Again, as shown in Chapter 2, Figure 2.5 the lateral acceleration a vehicle can obtain decreases significantly with decreasing velocity so it may not be desirable to decelerate the vehicle down to a stationary position. Moreover, in the case of a traffic scenario where an oncoming vehicle approaches from the opposite direction, slowing down the vehicle to a stationary position too early will most certainly end up in a collision.

Bearing the above in mind, it was decided that a suitable maneuver for the simulation based approach is to request a maximum steering signal and a maximum braking signal as an initial intervention, and then at a certain *switching velocity* v_s, switch to a steering only maneuver. An optimal switching velocity cannot intuitively be observed and can vary with other parameters such as initial velocity of the host vehicle, overlap with a threat, velocity or heading of a threat object, etc. It was therefore decided to run, for each simulation setup, a number of simulations with different switching velocities ranging between $0\,\mathrm{km\,h^{-1}}$ and the initial velocity of the host vehicle, sampled with a $5\,\mathrm{km\,h^{-1}}$ interval. The switching velocity that yielded the shortest TTR for each simulation setup was then chosen.

Let's recall from Chapter 2 that in order to maintain passenger comfort the lateral acceleration should be kept within $2.5\,\mathrm{m\,s^{-2}}$. For the simulation based approach, an attempt was made to limit the lateral acceleration to $2.5\,\mathrm{m\,s^{-2}}$ by regulating it with a PID controller when that limit is exceeded. For higher initial velocities, the lateral acceleration in some cases exceeds the limit quite significantly but only for a short period of time before the PID manages to regulate the steering angle.

3.2 Traffic scenarios

Car accidents occur in a variety of different traffic scenarios, some of which have been classified into specified categories and are commonly used in the automotive industry to benchmark safety system. For the application of this thesis, four common traffic scenarios have been chosen to evaluate and demonstrate the performance of a combined braking and steering maneuver. These traffic scenarios include: stationary obstacle, oncoming vehicle, vehicle cut-in and pedestrians, and are demonstrated in Figure 3.1.

3.2.1 Stationary obstacle on the road

Traffic scenarios involving collisions between moving vehicles and stationary obstacles are good abstractions of emergency traffic scenarios because they highlight the capabilities of the host vehicle. A traffic scenario of this kind is illustrated in Figure 3.1a, where a stationary threat vehicle is located in front of a moving host vehicle. For this traffic scenario, it is interesting to examine how combined braking and steering maneuver performs for different overlaps with a threat vehicle and compare the results with the performance of braking only, and steering only maneuvers.

Using a reference simulation environment, it is possible to simulate traffic scenarios where a threat vehicle has been placed in front of an host vehicle with a certain overlap and where an intervention is triggered at a certain time. In order to identify the latest TTC at which an intervention could successfully avoid a collision for a range of different overlaps and initial velocities, one would have to sweep for four

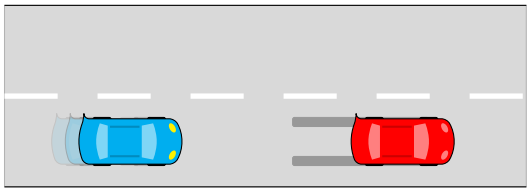

(a) Stationary obstacle on the host vehicle's lane.

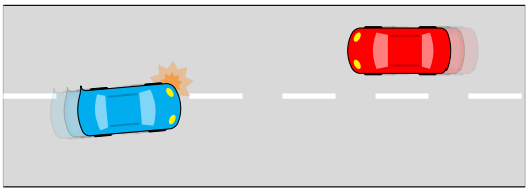

(b) The host vehicle leaves to the opposite lane while an oncoming threat vehicle approaches from the opposite direction.

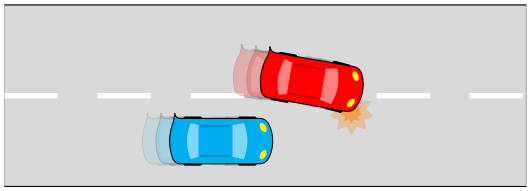

(c) The threat vehicle cuts-in in front of the host vehicle.

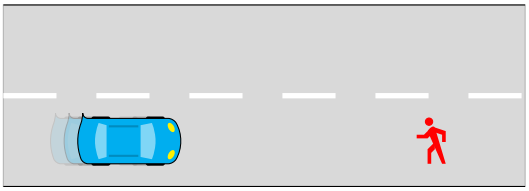

(d) A pedestrian crosses the road in front of the host vehicle.

Figure 3.1: Considered traffic scenarios. In the above figures, the blue and the red vehicles represent the host and the threat vehicles, respectively.

variables, initial velocity, overlap, triggering TTC and switching velocity v_s. This would not be feasible in a complex simulation environment such as the one used for this application. Instead, it was decided to use the reference simulation environment to only sweep for two variables, initial velocities v_0 and switching velocities v_s of the host vehicle, since these two variables affect the dynamics of the host vehicle. The remaining two variables, overlap and TTR, only affect the stationary threat vehicle and were obtained mathematically. This way, the shortest TTR was obtained for a broad range of overlaps and initial velocities of the host vehicle.

Simulation results where TTR is plotted over a range of initial velocities are shown in Figure 3.2 and Figure 3.3 for a 40 % overlap and a 100 % overlap, respectively. The performance of a combined braking and steering maneuver is compared with the performance of interventions where steering and braking are applied separately. The relationship between the initial velocity and TTR for which a collision can only be avoided with a combined maneuver, but not with the independent maneuvers, is marked with a gray color.

Equivalent results for a broader range of overlaps can be found in appendix A, in Figure A.1 (5 %), Figure A.2 (10 %), Figure A.3 (15 %), Figure A.4 (25 %), Figure A.5 (50 %) and Figure A.6 (75 %).

These results suggest that for lower initial velocities, there are no benefits of using steering and braking in combination over using braking only. In these situations,

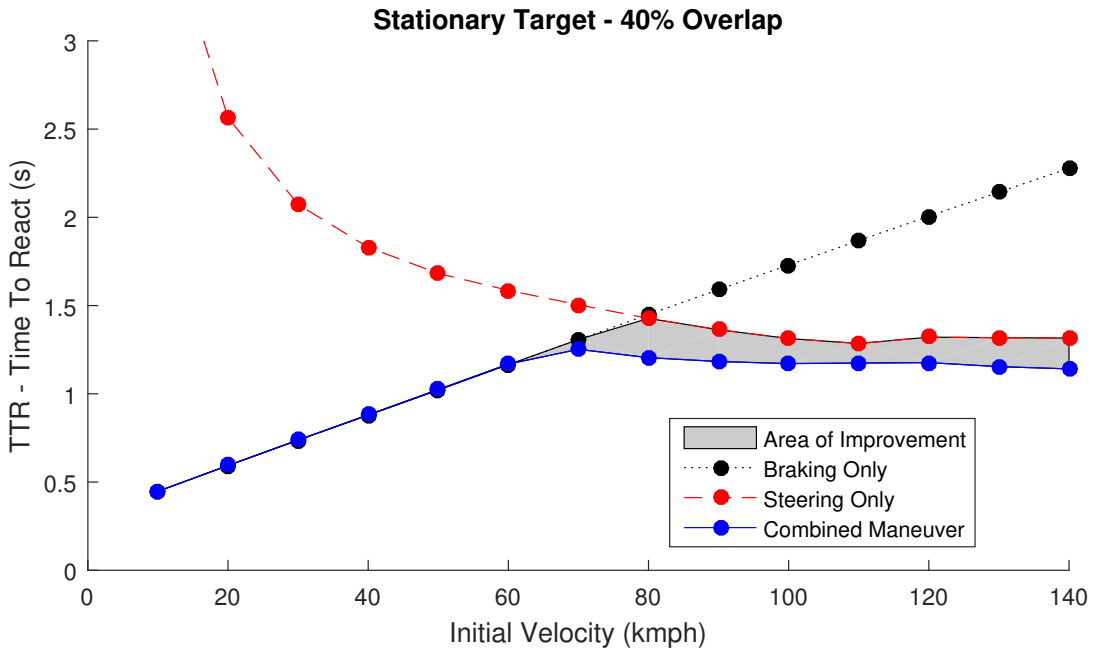

Figure 3.2: This figure demonstrates the minimum time needed to react in order to avoid a collision with a stationary obstacle with 40 % overlap in front of the host vehicle, for a range of initial velocities of the host vehicle. The gray area marks the relationship between velocity and TTR for which a collision can be avoided with a combined maneuver but not with steering only or a braking only intervention.

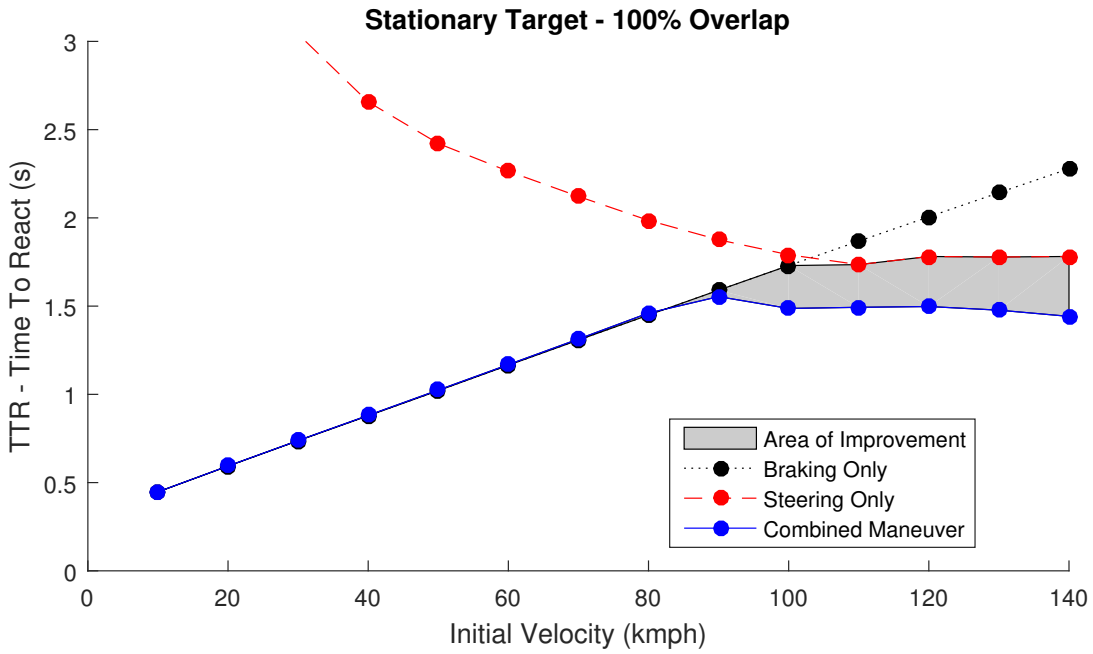

Figure 3.3: This figure demonstrates the minimum time needed to react in order to avoid a collision with a stationary obstacle with 100 % overlap in front of the host vehicle, for a range of initial velocities of the host vehicle. The gray area marks the relationship between velocity and TTR for which a collision can be avoided with a combined maneuver but not with steering only or a braking only intervention.

braking only maneuvers are very effective and cannot be outperformed by maneuvers that leverage steering as well. However, with increasing initial velocity, maneuvers that leverage steering start to become significantly more effective as the distance needed to decelerate a vehicle down to stationary increases exponentially with velocity [20]. Moreover, in all cases where a steering only maneuver performs better than a braking only maneuver, the steering only maneuver can be outperformed by a combined braking and steering maneuver.

In order to benchmark these results against AEB systems, triggering times of a reference AEB system (measured in TTC at intervention) were recorded for a variety of different cases and an attempt was made to avoid the collision with a combined braking and steering maneuver. The results are demonstrated in Table 3.1 for a range of different initial velocities and overlaps where the performance of the reference AEB systems is compared to a steering only, and a combined braking and steering maneuver.

v_0^{host}	AEB	Steering Only					Steering and Braking				
		≤ 25	40	50	75	100	≤ 25	40	50	75	100
10	✓	✗	✗	✗	✗	✗	✓	✓	✓	✓	✓
20	✓	✗	✗	✗	✗	✗	✓	✓	✓	✓	✓
30	✓	✗	✗	✗	✗	✗	✓	✓	✓	✓	✓
40	✓	✗	✗	✗	✗	✗	✓	✓	✓	✓	✓
50	✓	✓	✗	✗	✗	✗	✓	✓	✓	✓	✓
60	✗	✓	✗	✗	✗	✗	✓	✓	✓	✓	✓
70	✗	✓	✗	✗	✗	✗	✓	✓	✓	✓	✓
80	✗	✓	✗	✗	✗	✗	✓	✓	✓	✗	✗
90	✗	✓	✗	✗	✗	✗	✓	✓	✓	✗	✗
100	✗	✓	✗	✗	✗	✗	✓	✓	✓	✗	✗
110	✗	✓	✗	✗	✗	✗	✓	✓	✓	✗	✗
120	✗	✓	✗	✗	✗	✗	✓	✓	✓	✗	✗
130	✗	✓	✗	✗	✗	✗	✓	✓	✓	✗	✗
140	✗	✓	✗	✗	✗	✗	✓	✓	✓	✗	✗
$(km\,h^{-1})$		(% overlap)					(% overlap)				

Table 3.1: A successful evasive maneuver is denoted with check mark ✓ and a collision is denoted with a cross ✗ . For each velocity, an intervention is triggered at the same TTC as the reference AEB system would have applied the vehicle's brakes at. Collisions that can be avoided with a combined braking and steering maneuver but not with the reference AEB system nor with a steering only maneuver are shaded with a light blue background.

In Table 3.2, optimal switching velocities for different overlaps and different initial velocities of the host vehicle are presented. For higher overlaps and lower initial velocities, the optimal switching velocity is zero. That means that the optimal control strategy is to apply full braking until the vehicle reaches a stationary position. When the optimal switching velocity is on the other hand equal to the initial velocity, the optimal control strategy is to never apply the brakes but to steer only the entire time. Interestingly, the latter is never the case. Instead, for smaller overlaps and higher velocities, the optimal switching velocity is just slightly lower than the initial velocity. For example, one can observe from the table that for 5 % overlap and an initial velocity of $70\,km\,h^{-1}$ the optimal switching velocity is $65\,km\,h^{-1}$. In this case the control strategy to avoid the collision is to maneuver the vehicle laterally as quickly as possible until it no longer overlaps laterally with the threat. In order to build lateral acceleration and lateral velocity up as quickly as possible, decreasing the speed of the vehicle is not desirable. However, by leveraging the added steering wheel torque obtained by applying the brakes while steering, as discussed in Chapter 2, one can build up lateral acceleration faster by applying the brakes for a short

amount of time without compromising a significant amount of speed.

3.2.2 Oncoming vehicle from the opposite lane

A traffic scenario involving an oncoming vehicle is illustrated in Figure 3.1b where the host vehicle drifts towards an oncoming vehicle in the adjacent lane. What makes this scenario particularly interesting is that it is one of the scenarios that vehicles are benchmarked against under Euro NCAP ratings. Vehicles are tested under a series of use cases where parameters such as lateral acceleration, lateral velocity and initial velocity vary. Unlike the stationary scenario, parameters that define the oncoming scenario are not orthogonal, i.e. they are highly dependant on one another through the dynamics of the vehicle. For example, changing the initial velocity of the host vehicle affects its lateral acceleration and lateral velocity. This makes the oncoming scenario both harder and less practical to abstract mathematically in a way that would result in a reduction of parameters needed to sweep for, as was done with the stationary scenario. Instead, use cases of the oncoming scenario that

$\mathbf{v_0^{host}}$		**Optimal Switching Velocity**							
	OL:	5 %	10 %	15 %	25 %	40 %	50 %	75 %	100 %
10		0	0	0	0	0	0	0	0
20		0	0	0	0	0	0	0	0
30		0	0	0	0	0	0	0	0
40		25	0	0	0	0	0	0	0
50		40	30	0	0	0	0	0	0
60		55	40	35	35	0	0	0	0
70		65	60	50	45	40	0	0	0
80		75	70	60	60	55	50	35	0
90		85	80	75	70	65	60	55	45
100		95	90	90	80	75	75	65	60
110		105	100	100	95	90	85	75	70
120		115	110	110	105	100	100	85	85
130		125	120	120	115	110	110	105	95
140		135	135	130	125	120	120	120	115
$(\mathrm{km\,h^{-1}})$		$(\mathrm{km\,h^{-1}})$							

Table 3.2: Optimal switching velocities v_s. Velocities at which the input combination is switched from combined braking and steering to steering only, in order to obtain an optimal evasive trajectory when approaching a stationary obstacle on the road.

have been tested against a reference eLKA system in the RSE were identified and reproduced in a simulation. The performance of a combined braking and steering maneuver was then compared to the performance of a steering only maneuver by measuring the minimum TTR for which a collision could be successfully avoided, not accounting for any clearance between the two vehicles. The identified use cases are listed in Table 3.3, each labelled with alphabetic letters ranging between A and M. The columns are as follows: v_{lat} is the lateral velocity, a_{lat} lateral acceleration and v_0 velocity, all measured at the point of intervention. The lateral and longitudinal offsets are the lateral- and longitudinal distances between the two vehicles in the inertial frame at the point of intervention and v_s is the optimal switching velocity. The host vehicle was simulated in the RSE while the movement of the oncoming vehicle was modelled mathematically to calculate the optimal switching velocity and the TTR.

U.C.	$\mathbf{v_{lat}}$	$\mathbf{a_{lat}}$	$\mathbf{v_s}$	$\mathbf{v_0}$		**Offset**	
				host	threat	lat.	long.
A	0.2	0	65	70	20	-0.10	52.14
B	0.3	0	65	70	20	-0.23	51.90
C	0.4	0	65	70	20	-0.37	52.13
D	0.5	0	65	70	20	-0.51	52.52
E	0.6	0	65	70	20	-0.64	52.40
F	0.3	0.3	65	90	20	-0.20	51.34
G	0.4	0.4	65	90	20	-0.32	51.39
H	0.5	0.5	65	90	20	-0.44	51.33
I	0.6	0.6	65	90	20	-0.56	51.36
J	0.3	0.3	65	110	20	-0.16	51.37
K	0.4	0.4	70	110	20	-0.26	51.38
L	0.5	0.5	70	110	20	-0.37	51.40
M	0.6	0.6	65	110	20	-0.48	51.37
	$(\mathrm{m\,s^{-1}})$	$(\mathrm{m\,s^{-2}})$	$(\mathrm{km\,h^{-1}})$	$(\mathrm{km\,h^{-1}})$	$(\mathrm{m\,s^{-1}})$	(m)	

Table 3.3: Identified use cases of the oncoming scenario where v_{lat}, a_{lat} and v_0 are lateral velocity, lateral acceleration and initial velocity of the host vehicle at the point of intervention and the offset are the lateral and longitudinal distance between the two vehicles in the inertial frame at the point of intervention. v_s is the optimal switching velocity.

The performance of the two maneuvers, the braking and steering maneuver and the steering only maneuver, are compared in Figure 3.4 for each use case.

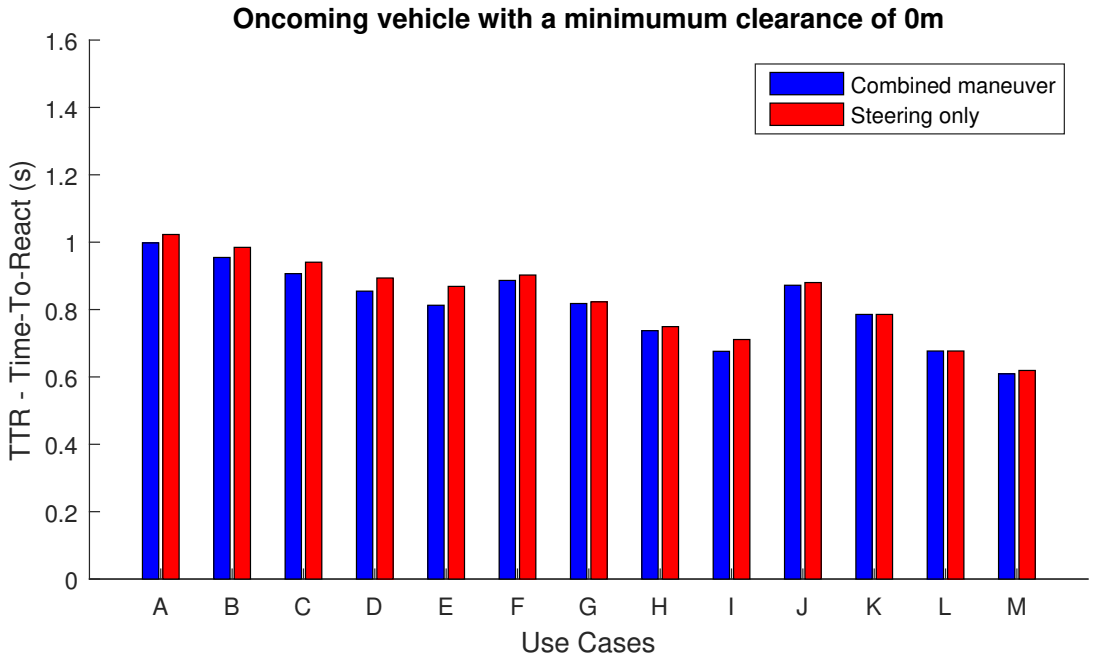

Figure 3.4: Bar plot illustrating TTR for steering only maneuvers and combined braking and steering maneuvers for the cases defined in Table 3.3

For most of the referred use cases, a collision could be avoided with a lower TTR by applying a combined braking and steering maneuver over a steering only maneuver. However, the gain is hardly significant as compared to the stationary scenario. Simulation results where the minimum clearance accounted for between the two vehicles is 0.1 m and 0.2 m respectively can be found in Figure A.8 and Figure A.9 respectively in appendix A.

For comparison, another set of simulations were performed where the performance of a combined braking and steering maneuver was compared to a reference eLKA system. In this set of simulations, both the host vehicle and the threat vehicle were simulated in the RSE. Previous simulations performed for a reference eLKA system were replicated using a combined braking and steering maneuver instead of a steering only maneuver, with the objective to delay the intervention as much as possible while keeping at least the same clearance between the two vehicles. The results are demonstrated in Table 3.4 .

v_{lat}	a_{lat}	v_0		Avoided		Improvement
		host	threat	eLKA	Combined	
0.2	0	70	20	✓	✓	50.3
0.3	0	70	20	✓	✓	49.3
0.4	0	70	20	✓	✓	95.4
0.5	0	70	20	✓	✓	125.6
0.6	0	70	20	✓	✓	150.7
	($m\,s^{-2}$)	($km\,h^{-1}$)	($m\,s^{-1}$)			(ms)

Table 3.4: Combined braking and steering maneuver compared to a reference eLKA system. The last column, improvement, denotes how much an intervention can be delayed while still avoiding the collision with at least the same clearance as can be done with the reference eLKA system.

3.2.3 Pedestrian crossing the road

Collisions with *Vulnerable Road Users* (VRUs) is one the most important concerns of road safety. Pedestrians and cyclists are involved in 26 % of all road traffic fatalities, according to the *World Health Organization* (WHO) [15]. An illustration of pedestrian scenario can be seen in Figure 3.1d. One of the main problems of these scenarios is the randomness of intended path of the VRUs, which is very difficult to predict. However, if the path of the VRUs can be predicted accurately a small change in heading can avoid the collision.

Just like the oncoming scenario that was discussed in the previous section, a traffic scenario involving a pedestrian is one of the scenarios vehicles are tested against during Euro nCAP ratings. During the ratings, the pedestrian is modelled as an object crossing the road with a constant velocity. This scenario can be seen as an extension to the stationary scenario, with the added complexity of a constant lateral velocity of the threat, resulting in a changing lateral overlap over time.

For this scenario a combined braking and steering maneuver can be performed with two different control strategies, either to steer in front of the pedestrian, in which case the overlap with the threat increases over time, or to steer behind him which results in a decreasing overlap over time. The lateral overlap between the vehicle and the center of the pedestrian at time of collision, assuming that no action is taken to avoid the collision, is known as the hitpoint. The combination between the hitpoint, the velocities of the pedestrian and the velocity of the vehicle determines at which TTC the pedestrian starts crossing the road.

In order to compare the performance of a combined braking and steering maneuver to braking only and steering only maneuvers, a similar methodology was applied as was applied to the stationary scenario. The RSE was used to simulate a series

of trajectories of the vehicle for a range of different initial velocities and switching velocities while the pedestrian was modelled and simulated mathematically. The simulation of the pedestrian was repeated for range of different hitpoints and two different walking velocities, $5\,\mathrm{km\,h^{-1}}$ and $8\,\mathrm{km\,h^{-1}}$. Additionally, the simulation was repeated for the two different control strategies of steering either in front of the pedestrian or behind him. To do this, an assumption was made that the vehicle's dynamics were symmetric along the longitudinal axis. With that in mind, instead of repeating the simulation of the vehicle in the RSE where the vehicle would steer in both directions, the simulation of the pedestrian was repeated where he was placed on the both sides of the lane crossing from both both directions.

Figure 3.5 and Figure 3.6 show how a combined braking and steering maneuver performs compared to braking only and steering only maneuvers while steering in front of the pedestrian and behind him respectively. In the figures, the pedestrian is walking at $5\,\mathrm{km\,h^{-1}}$ and the hitpoint is at 50 % overlap.

Comparing Figure 3.5 and Figure 3.6 indicates that steering behind the pedestrian is a significantly more effective control strategy than steering in front of him. Obviously, in real traffic scenarios, other factors such as probabilities of different reactions of the pedestrian to an approaching vehicle may play an important role. However in this comparison, a constant velocity of the pedestrian while crossing the road is assumed.

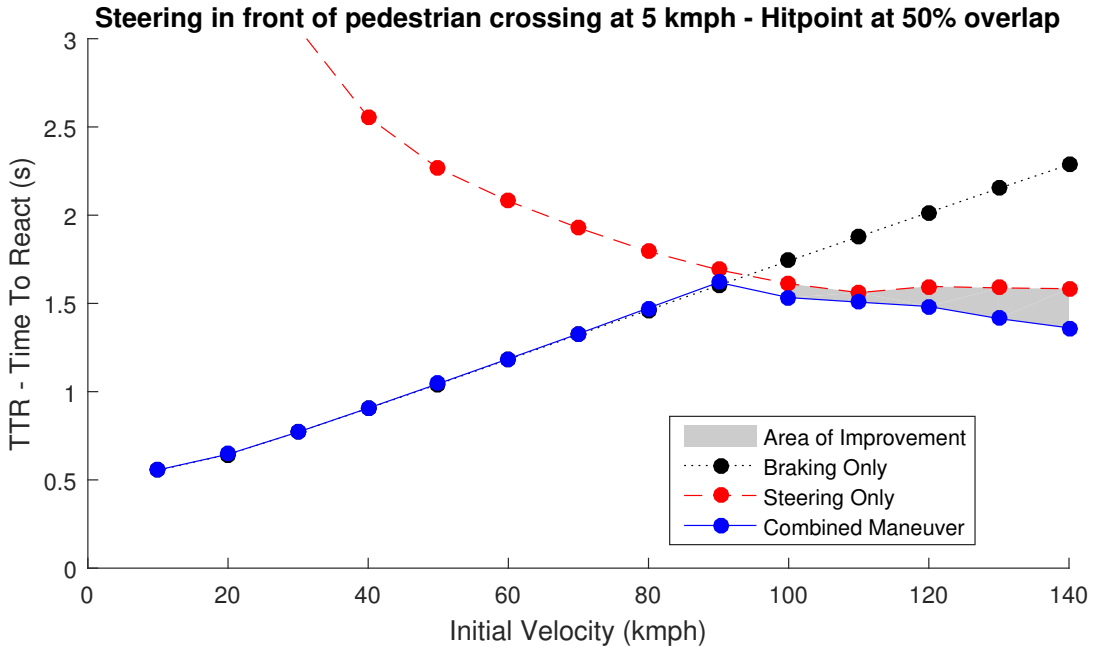

Figure 3.5: Combined braking and steering maneuver compared to braking only and steering only maneuvers when attempting to steer in front of a pedestrian crossing the road at $5\,\mathrm{km\,h^{-1}}$, approaching a collision with a hitpoint at 50 % overlap. The combination of TTR and initial velocity highlighted within the gray area is where a collision can be avoided with a combined braking and steering maneuver but not with braking only or steering only maneuvers.

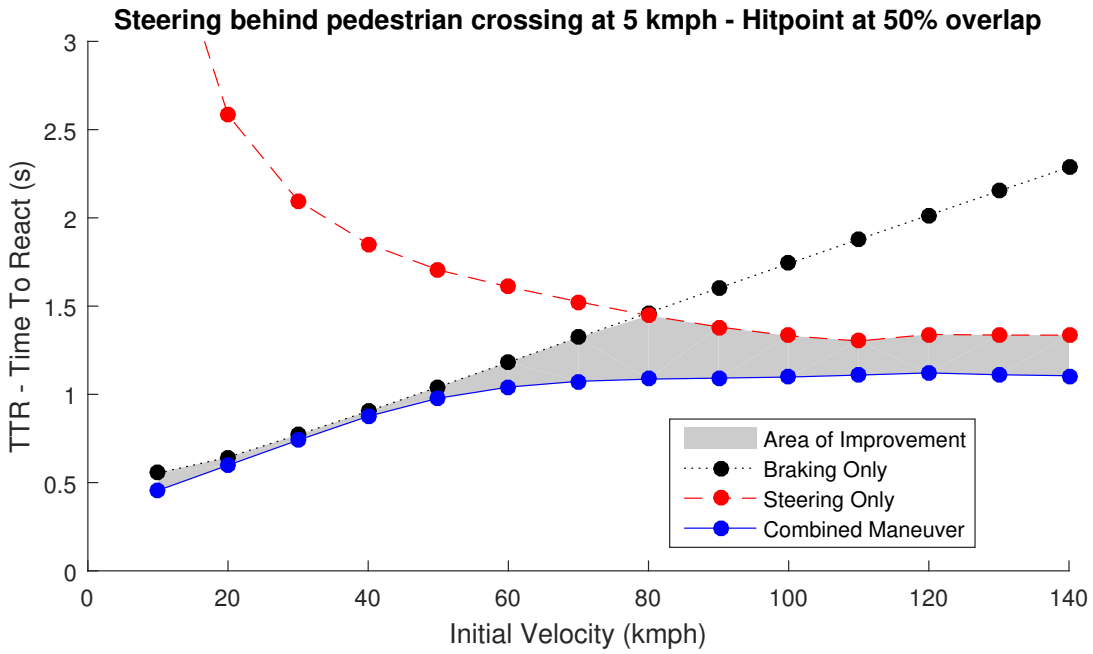

Figure 3.6: Combined braking and steering maneuver compared to braking only and steering only maneuvers when attempting to steer behind a pedestrian crossing the road at $5\,\mathrm{km\,h^{-1}}$, approaching a collision with a hitpoint at 50 % overlap. The combination of TTR and initial velocity highlighted within the gray area is where a collision can be avoided with a combined braking and steering maneuver but not with braking only or steering only maneuvers.

Figures that demonstrate simulation results for different hitpoints and walking speeds of the pedestrian, as described in Table 3.5, can be found in appendix A.

Walking speed	**Hitpoint**	**Control Strategy (steering direction)**	
		In front of pedestrian	Behind pedestrian
$5\,\mathrm{km\,h^{-1}}$	25 %	Figure A.10	Figure A.11
$5\,\mathrm{km\,h^{-1}}$	50 %	Figure 3.5	Figure 3.6
$5\,\mathrm{km\,h^{-1}}$	75 %	Figure A.12	Figure A.13
$8\,\mathrm{km\,h^{-1}}$	25 %	Figure A.14	Figure A.15
$8\,\mathrm{km\,h^{-1}}$	50 %	Figure A.16	Figure A.17
$8\,\mathrm{km\,h^{-1}}$	75 %	Figure A.18	Figure A.19

Table 3.5: Figures that demonstrate the performance of a combined braking and steering maneuver with respect to a traffic scenario involving a pedestrian crossing the road. The referred figures can be found in appendix A.

3.2.4 Vehicle cut-in scenario

Cut-in scenario is another critical scenario under Euro NCAP ratings against which vehicles are benchmarked. The scenario is defined as a threat vehicle suddenly emerging in host-lane from the adjacent lane, where both vehicles are driving in the same direction. Figure 3.1c shows an illustration of a cut-in scenario.

In this scenario, the threat vehicle is exposed to both longitudinal- and lateral dynamics which makes it more difficult to abstract mathematically than the other scenarios considered in this thesis. Therefore for this scenario only one set of simulations were performed. In this set of simulations, both the host vehicle and the threat vehicle were simulated in the RSE. Primarily, a range of simulations were performed, with different speeds of the host vehicle and the threat vehicle, to measure the triggering instance and clearance between the two vehicles for a reference AEB system. Subsequently, the same simulations were repeated iteratively for a combined braking and steering maneuver with the objective to delay the intervention as much as possible, while maintaining at least the same clearance between the two vehicles.

Comparisons of combined maneuvers and reference AEB systems for the vehicle cut-in scenario are presented in Table 3.6. From the table it could be inferred that, the systems leveraging combined braking and steering maneuvers provide some improvement in all the cases where the reference AEB systems can avoid a collision for cut-in scenarios. In addition to that, combined braking and steering maneuver outperforms reference AEB systems for the case where both vehicles have high velocities.

v_0		Avoided		Improvement
host	threat	AEB	Combined.	
50	20	✗	✗	0
50	40	✓	✓	5.1
70	20	✗	✗	0
70	40	✗	✗	0
70	60	✓	✓	3.6
90	40	✗	✗	0
90	60	✓	✓	59.1
90	80	✓	✓	2.8
120	90	✓	✓	63.0
120	110	✗	✓	31.2
($\mathrm{km\,h^{-1}}$)	($\mathrm{m\,s^{-1}}$)			(ms)

Table 3.6: Comparison of braking maneuvers and combined maneuvers in terms of TTC for Cut in Scenario.

4

Reachability Analysis

Formal analysis has recently gained interest among researchers for threat assessment. Such methods have been used extensively by computer scientists, specially in software and hardware engineering. The core idea behind formal analysis is to derive correct-by-design control systems by performing mathematical analysis which can contribute to the system's reliability and robustness [7]. Formal analysis approaches can be divided into two categories, i) logic based approaches and ii) set based approaches. As the name suggests, logic-based formal analysis methods leverage logical sentences to formalize requirements, in order to verify the design of the system. In set-based approaches, requirements are proposed according to the accepted and forbidden input sets and configuration sets of the system.

In addition to threat assessment, reachability analysis can be used for applications such as performance assessment of control strategies, scheduling, controller synthesis, etc. Reachability analysis is the subject of finding all possible state combinations a system can reach where some system properties such as dynamics, parameters, noise, states or inputs are not known but bounded within an admissible uncertainty.

In this chapter, we describe how reachability analysis was used to predict the set occupancy of vehicle using the model derived in Chapter 2.

4.1 Set Representations for Reachability Analysis

When performing reachability analysis, reachable sets must be represented with mathematical expressions. In the literature, there are many different representations available to represent reachable sets, such as intervals, ellipsoids, polytopes and zonotopes, each with different characteristics, pros and cons. Moreover, there are generally four main mathematical set operation necessary for reachability analysis:

- Linear Transformation
- Minkowski sum
- Convex hull

- Intersection

It is worth mentioning that the choice of an appropriate set representation for reachability analysis also depends on the intended application. A few set representations considered in this thesis are described below.

4.1.1 Polytopes

One way to represent reachable sets of linear systems is with polytopes. Polytopes are defined as the convex hull of its vertices and can be used to represent a set in any dimension. There are two common ways to represent polytopes, either by the intersection of half spaces that bound the polytope's facets or as the convex hull of the polytope's vertices. The former is known as *H-Representation* and the latter as *V-Representation*. An H-represented zonotope is defined as follows,

$$P = \left\{ x \in \mathbb{R}^n \;\middle|\; \mathbf{C}x \leq \mathbf{d},\ (\mathbf{C}, \mathbf{d}) \in \mathbb{R}^{n_h \times n} \times \mathbb{R}^{n_h} \right\}, \tag{4.1}$$

where n_h and n are the number of halfspaces defined for each dimension and the number of dimensions, respectively. V-represented polytopes are commonly used for forward reachability analysis of linear systems due to mathematical advantages that come along with them. A major problem with V-represented polytopes reachability analysis is that they suffer from the curse of dimensionality as the number of their vertices can easily grow exponentially with the number of their dimensions. This makes v-represented polytopes only feasible as representations for reachable sets in systems where the number of states are limited to around four states. Illustrations of V-representations and H-representations are shown in Figure 4.1.

4.1.2 Zonotopes

Zonotopes are special cases of polytopes that are centrally symmetric. Due to the symmetrical nature of zonotopes, mirrored information can be lumped together which makes it possible to represent sets with a so called *G-representation*. A G-representation of a zonotope consists of a center point and set of vectors known as *generators*. A zonotope is defined as every possible linear combination of the generator matrix and a set of line segments ξ where $\xi_i \in [-1, 1]$. This linear combination is then added to the coordinate of a center point $\mathbf{c}$, as shown in the following equation,

$$\mathcal{Z} = \left\{ \mathbf{c} + \mathbf{G}\xi \;\middle|\; \|\xi\|_\infty \leq 1,\ (\mathbf{G}, \mathbf{c}, \xi) \in \mathbb{R}^{n \times n_g} \times \mathbb{R}^n \times \mathbb{R}^{n_g} \right\}, \tag{4.2}$$

where $\mathbf{c}$ is the center point and $\mathbf{G} = \begin{bmatrix} g_1 & \dots & g_{n_g} \end{bmatrix}$ is a set of generators g_i.

An illustration of a G-representation is shown in Figure 4.2.

The advantage of G-representations over the H- and V-representations, is that fewer data is needed to represent sets. This paves the way for improved scalability where

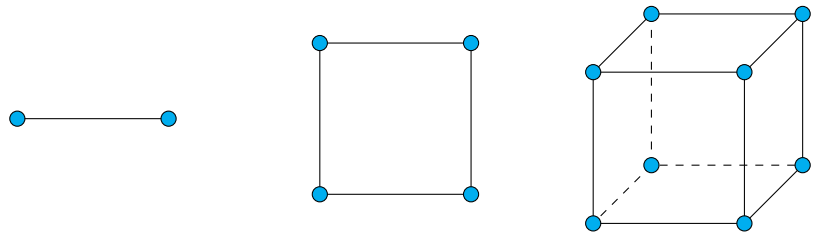

(a) V-Representation. The polytope is defined as the convex hull of all vertices.

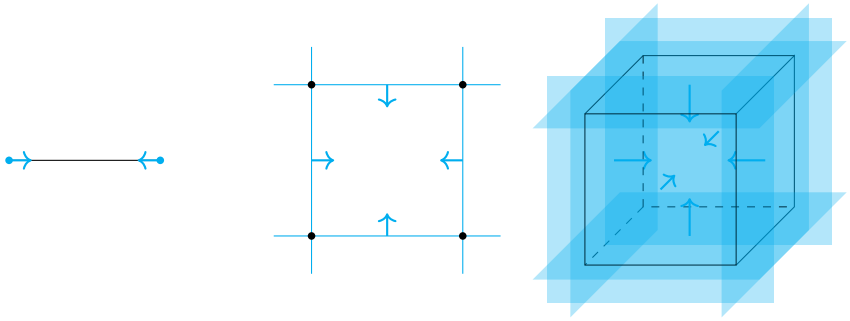

(b) H-Representation: The polytope is defined as intersection of the half spaces bounded by the facets of the polytope.

Figure 4.1: Illustrations of polytope representations.

the complexity of problems tends to grow linearily with the number of states instead of exponentially. Zonotopes are closed under *Minkowski addition* and *linear mapping* which are fundamental operations used in reachability analysis. The computation of a convex hull of two zonotopes does not generally result in another zonotope, except in the case of two identical zonotopes, although the convex hull can be tightly overapproximated with a zonotope. Zonotopes are not closed under intersection.

In the following sections, other varieties of zonotopes will be introduced as well. To avoid confusion, zonotopes that are explicitly of the type described in equation (4.2) are referred to as *linear zonotopes*.

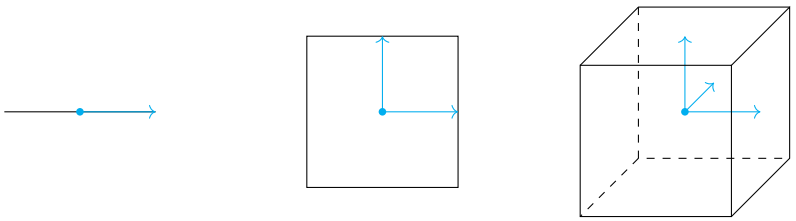

Figure 4.2: Illustration of the G-Representation of zonotopes. The zonotope is defined by all possible linear combination of the generators, which are noted with blue arrows, and a set of line segments ξ such that $\xi_i \in [-1, 1]$.

4.1.3 Constrained Zonotopes

Constrained zonotopes were introduced in 2016 in [19] and are defined as follows,

$$\mathcal{Z}_c = \left\{ \mathbf{c} + \mathbf{G}\xi \;\middle|\; \|\xi\|_\infty \leq 1,\ \mathbf{A}\xi = \mathbf{b}, (\mathbf{G}, \mathbf{c}, \mathbf{A}, \mathbf{b}) \in \mathbb{R}^{n \times n_g} \times \mathbb{R}^n \times \mathbb{R}^{n_c \times n_g} \times \mathbb{R}^{n_c} \right\}, \tag{4.3}$$

where n is the number of dimensions, n_g is the number of generators and n_c is the number of constraints.

As an upgrade to linear zonotopes, constrained zonotopes are very powerful and can in many ways be considered as a combination of polytopes and zonotopes, as they inherit all properties from zonotopes and many properties from polytopes. Unlike linear zonotopes, constrained zonotopes are not necessarily centrally symmetric. Note that in equation (4.3) the notation

$$\mathbf{A}\xi = \mathbf{b}$$

is an equality constraint but not an inequality constraint as one might expect. This can be explained by the fact that when constraints are added to the constrained zonotope as rows to $\mathbf{A}$ and $\mathbf{b}$, corresponding generators of length zero are added as well. The added zero-generators do not affect the shape of the underlying zonotope. They do however come along with corresponding line segments $\xi_i \in [-1, 1]$, which act as slack variables and are used to formulate the constraints as equality constraints.

4.1.4 Other varieties of zonotopes

Zonotope bundles were introduced in [4] and are defined as the intersection of a set of zonotopes, such that:

$$\mathscr{L}^\cap = \left\{ \bigcap_{i=1}^{s} \mathcal{Z}_i \;\middle|\; \mathcal{Z}_i \in \mathscr{L} \right\}, \tag{4.4}$$

where $\mathscr{L}$ is a finite set of zonotopes.

Zonotope bundles are useful, for example, for applications that require intersections of sets since linear zonotopes are not closed under intersection. Note though, that constrained zonotopes have perhaps made zonotope bundles outdated after their introduction in 2016. When representing an intersection of two linear zonotopes with a zonotope bundle $\mathscr{L}^\cap$, the intersection is not explicitly computed. Instead, the underlying zonotopes are stored in a set $\mathscr{L}$. When performing operations on the bundle $\mathscr{L}^\cap$, those operations are projected to equivalent operations that are performed separately on the zonotopes $\mathcal{Z}_i \in \mathscr{L}$. Linear transformations, intersections and facet liftings can be computed exactly and other operations such as the Minkowski additions, convex hulls and box enclosures are overapproximated.

Polynomial zonotopes were introduced in [3] as a way to represent non-convex reachable sets of non-linear systems. Unlike linear zonotopes, where a set is defined as

all possible linear combination of a generator matrix $\mathbf{G}$ and a set of line segments ξ, where $\xi_i \in [-1, 1]$, sets represented with polynomial zonotopes are defined as a polynomial combination of generator matrices and line segments. Polynomial zonotopes are defined as follows,

$$\begin{aligned}\mathcal{PZ} = \{ c + \sum_{\mathbf{j=1}}^{\mathbf{p}} \beta_j f^{([1],j)} + \sum_{\mathbf{j=1}}^{\mathbf{p}} \sum_{\mathbf{k=j}}^{\mathbf{p}} \beta_j \beta_k f^{([2],j,k)} \\ + \cdots + \sum_{\mathbf{j=1}}^{\mathbf{p}} \sum_{\mathbf{k=j}}^{\mathbf{p}} \cdots \sum_{\mathbf{m=l}}^{\mathbf{p}} \beta_j \beta_k \cdots \beta_m f^{([n],j,k,\cdots,m)} \\ + \sum_{\mathbf{i=1}}^{\mathbf{q}} \gamma_j g^{(i)} \;\Big|\; \beta_i, \gamma_j \in [-1, 1],\end{aligned} \tag{4.5}$$

where, scalars β_i are termed as dependent factors since they affect multiplication with several generators, while scalars γ_i are called independent factors as they affect multiplication with only one generator.

4.2 CORA - A continuous reachability analyzer

CORA is an open source Matlab toolbox for reachability analysis, licensed under *GNU General Public License, version 3.0*. It is currently in active development and it comes with some interesting features and capabilities that are very promising for the application of this thesis. CORA supports several set representations including intervals, polytopes, zonotopes, zonotope bundles, constrained zonotopes and polynomial zonotopes, which makes CORA a flexible tool for applications that involve complexities such as nonlinear systems and hybrid systems.

CORA is capable of operating on a very high level. For example, a user can specify a set of continuous nonlinear differential equations along with a set of maximum error tolerances for each state and CORA will automatically linearize the system and make sure that linearization error limits are not exceeded.

Unless stated otherwise, we will in the following sections specifically discuss how CORA uses zonotopes for reachability analysis.

4.2.1 Non-linearities

Non-linearities are a huge problem within reachability analysis. Traditional linearization methods cannot generally be applied for set based methods since such approximations would have to represent the true system well enough, not only around a single point but within a whole set of values. Depending on the size of the set and on the significance of the non-linearities, representing a non-linear system with a linear system may not be feasible.

Furthermore, reachable sets of non-linear systems are not guaranteed to be convex, in which case a good representation cannot be obtained with convex set representation such as polytopes or zonotopes.

There are three main ways CORA represents reachable sets of nonlinear systems:

1. *Linearization.* Minor non-linearities can be approximated as linear functions using a first order Taylor expansion. By default, functions are linearized around the center point of the zonotope although other points can optionally be chosen as well.

2. *Splitting the sets.* If the linearization error exceeds a user defined threshold, CORA splits the zonotope into two zonotopes. This is suitable for modest non-linearities but may become problematic if the the reachable sets grow significantly over time, which can easily result in an exponential growth of split zonotopes.

3. *Polynomial zonotopes.* Polynomial zonotopes can be used in presence of significant non-linearities for which the derivation of reliable results with linear zonotopes is not feasible. The non-linear function must be Lipschitz continuous within the set. In this case, CORA performs an n^{th} order Taylor expansion of the nonlinear model in order to approximate it as a polynomial. Currently, only *quadratic zonotopes* (polynomial zonotopes of order two) are supported in CORA but the developers are working on an implementation of general polynomial zonotopes.

4.2.2 Hybrid systems and state constraints

Systems that consist of a combination of continuous dynamics and discrete dynamics are known as *hybrid systems.* A common textbook example of a system that is often modelled as a hybrid system is a bouncing ball, where the motion of the ball is described with continuous dynamics while in the air but the bounce-back, when the ball hits the ground, is approximated as a instantaneous event.

Reachability analysis of hybrid systems is not a trivial subject. One challenge is intersecting reachable sets with so called *guard sets.* When a reachable set reaches a guard set, an event is triggered that executes a transition from one continuous system to another. In the case of the bouncing ball, the guard set is the floor and the transition is an instantaneous switch from a negative velocity to a positive velocity.

As previously mentioned, linear zonotopes are not closed under intersection but zonotope bundles and constrained zonotopes are. In order to intersect reachable sets with guard sets, CORA uses either *zonotope bundles* or *constrained zonotopes* to represent reachable sets of hybrid systems.

State constraints are not explicitly mentioned in the CORA manual and they don't seem to be accounted for in the software. However, the core idea is the same as with hybrid systems. In order to apply state constraints to reachable sets the reachable sets need to be intersected with the state constraints on every time step and therefore they need to be represented with either zonotope bundles or constrained zonotopes.

4.3 Approach description

Recall that, the model described in Chapter 2 represented by equation (2.10) is a six state hybrid model, with an affine (2.11a) and a non-linear (2.11d) constraint. We faced some difficulties in performing formal analysis for this model, using different toolboxes. For example, one very popular toolbox amongst researchers in the control community is the *MPT3* toolbox [12]. This toolbox uses polytopes to calculate reachable sets for LTI systems, which presents scalability issues as mentioned earlier. Hence, the model (2.10) being a six state non-linear model prohibited the usage of this toolbox. This was the main contributing factor to use the CORA toolbox for formal analysis in this thesis, as it could efficiently handle non-linear system with higher number of states. As mentioned earlier, CORA can be used to calculate reachable sets of non-linear and hybrid systems. However, it is not possible to calculate constrained reachable sets as state constraints are not explicitly implemented in the toolbox. Therefore, we have used constrained zonotopes, to represent state and constraints and to calculate the reachable sets. It is not feasible to include non-linear state constraints while calculating reachable sets as constrained zonotope is an extension of linear zonotope. In addition to that, to reduce complexity we have only considered sets calculation for continuous non-linear system. The necessary changes made to the model to fulfill the requirements are discussed in this section.

4.3.1 Modelling approximation of the yaw rate by a polynomial

Figure 4.3a describes how the yaw rate varies with respect to lateral acceleration and velocity according to equation (2.10c). Clearly, it is evident that the function is highly nonlinear and does not follow Lipschitz continuity principle.

A function $f : X \to Y$ is said to be Lipschitz continuous if there exists a real constant $K \geq 0$ such that for all x_1 and x_2 in X, the following equation holds:

$$d_Y(f(x_1), f(x_2)) \leq K d_X(x_1, x_1) \tag{4.6}$$

where the 2 metric spaces are defined as (X, d_X) and (Y, d_Y) and, d_X and d_Y represent metrics on the set X and Y respectively, for further details see [9].

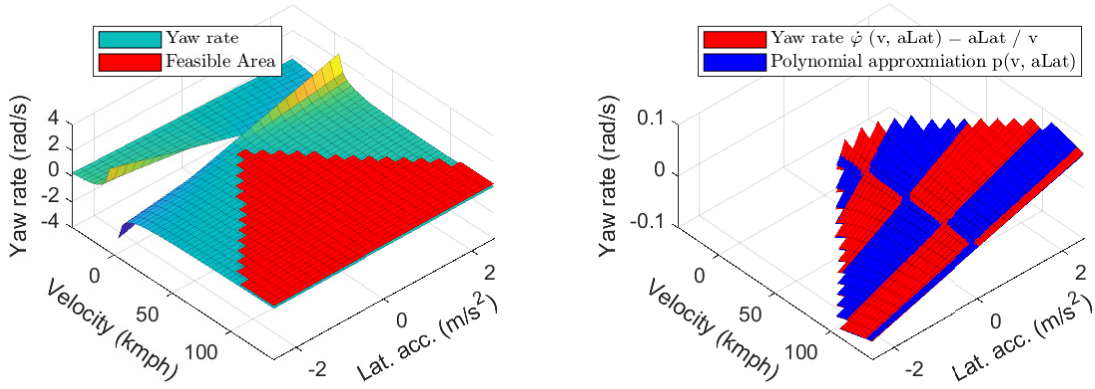

(a) Exact solution of $\dot{\varphi} = a_{lat}/v$ and the area satisfying the constraints (2.11a) and (2.11d).

(b) 1st order polynomial approximation using the relation in (4.7) and exact solution of $\dot{\varphi}(v, a_{Lat}) = a_{Lat}/v$ with affine constraints.

Figure 4.3: Polynomial approximation compared to the area of interest and exact solution of $\dot{\varphi}$.

In order to leverage the properties of polynomial zonotopes and satisfy the prerequisites of the Lipchitz continuity, we represent the yaw rate by a polynomial function of lateral acceleration and velocity. Nevertheless, the polynomial zonotopes are not closed under intersection, so, we have used constrained zonotope to derive reachable sets in this thesis work.

Different polynomial functions were calculated for different orders of mentioned variables using a Matlab script [14]. The calculated functions were then verified with the area of interest in order to obtain the best ,lowest order, fitting function. After checking a few different combinations, it was inferred that the area of interest could be approximated with a polynomial function of 1st order given as:

$$\dot{\varphi} \approx p_1 \cdot v \cdot a_{Lat} + p_2 \cdot a_{Lat} + p_3 \cdot v + p_4, \tag{4.7}$$

where, p_1, p_2, p_3 and p_4 are constants derived from [14]. Figure 4.3b shows now polynomial expression given in (4.7) approximates the exact solution and the area of interest quite accurately. Nevertheless, this approximation leads to a maximum over-approximation and under-approximation of 0.4 deg /s and 1.6 deg /s in yaw rate, respectively.

4.3.2 Constraint simplification

Using affine constraints on lateral acceleration as defined in (2.11a) can lead to a hybrid model as the heading rate dynamics changes below velocity $v = \frac{-c2}{c1}$, where $c1$ and $c2$ are constants from (2.11a). As mentioned earlier, the toolbox CORA can be used to calculate reachable sets for hybrid system, though in this project we have

only considered sets calculation for continuous non-linear system. Therefore, the affine constraint (2.11a) have been rewritten as a linear constraint such that:

$$|a_{lat}| \leq c_3 \cdot v, \tag{4.8}$$

where c_3 is calculated with respect to affine and saturated lateral acceleration constraints in the equations (2.11a) and (2.11b), respectively. In other words, the linear slope (c_3) is calculated using the maximum lateral acceleration obtained from the above mentioned constraints.

In Figure 4.4a, one can notice the extra relaxation in terms of lateral accelerations due to the change in constraint from affine to linear. This relaxation contributes to over-approximations when calculating different vehicle states such as the heading and the lateral position. Figure 4.4b shows the over-approximations due to the change in constraints from an affine (2.11a) to a linear (4.8) one, for different lateral acceleration saturation constraints. One can see that the lateral position difference increases for higher allowed lateral accelerations (i.e, maximum lateral acceleration allowed) which is due to the fact that the active region increases as well as the relaxation of lateral acceleration when using a linear constraint. The active region can be defined as the region where the lateral acceleration is constrained by the affine or the linear constraints in (2.7) and (2.11a), respectively. As mentioned earlier in 2, the GG-constraints are nonlinear constraints which determine the longitudinal deceleration dependence on the lateral acceleration of the vehicle following equation (2.11d). For the sake of simplification, in this thesis the maximum longitudinal deceleration is assumed to be a constant following the equation:

$$a_{long} = \sqrt{a_{max}^2 - a_{latMax}^2}, \tag{4.9}$$

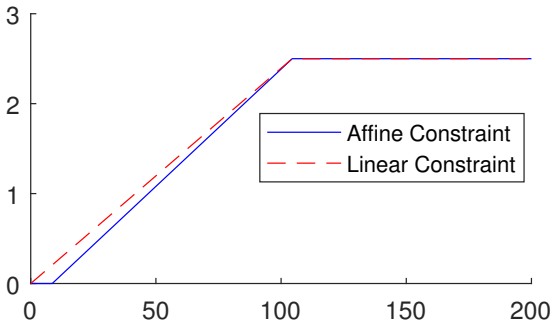

(a) Relaxation in lateral acceleration due to linear constraint with respect to affine constraints for a lateral acceleration saturation of $2.5\,\mathrm{m\,s^{-1}}$.

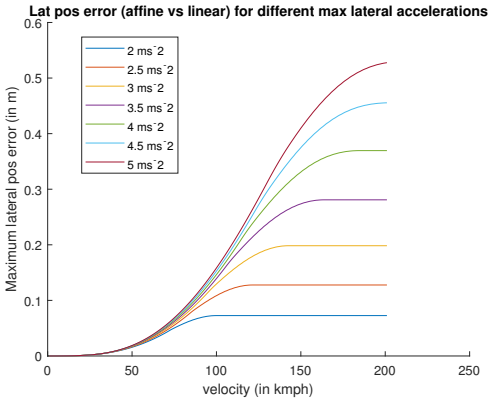

(b) Over-approximations in terms of lateral positions, due to change in lateral acceleration constraints from affine to linear using polynomial expression for yaw rate in equation (4.7).

Figure 4.4: Comparison between linear and affine lateral acceleration constraints

where a_{max} and a_{latMax} are the maximum acceleration of the vehicle and the saturation constraint on the lateral acceleration, respectively. Nevertheless, it is worth mentioning that this simplification introduces conservativeness on the longitudinal deceleration, though the difference is negligible, as the saturation constraint on lateral acceleration is quite low ($2.5\,\mathrm{m\,s^{-2}}$) in these results. This could be seen in Figure 2.7.

The model given in (2.10) can now be rewritten as :

$$\dot{p}_x = v \cdot \cos\varphi \tag{4.10a}$$
$$\dot{p}_y = v \cdot \sin\varphi \tag{4.10b}$$
$$\dot{\varphi} = p_1 \cdot v \cdot a_{Lat} + p_2 \cdot a_{Lat} + p_3 \cdot v + p_4 \tag{4.10c}$$
$$\dot{\varphi} = p \begin{bmatrix} v \cdot a_{lat} & a_{lat} & v & 1 \end{bmatrix}^T \tag{4.10d}$$
$$\dot{v} = u_1(t - \tau_1) \tag{4.10e}$$
$$\dot{a}_{lat} = j_{lat} \tag{4.10f}$$
$$\dot{j}_{lat} = u_2(t - \tau_2) \tag{4.10g}$$
$$\tag{4.10h}$$

subject to the following constraints:

$$|a_{lat}| \leq c_{Linear} \cdot v \tag{4.11a}$$
$$|a_{lat}| \leq 2.5\,\mathrm{m\,s^{-2}} \tag{4.11b}$$
$$v \geq 0 \tag{4.11c}$$
$$a_{long} = \sqrt{a_{max}^2 - 2.5^2} \tag{4.11d}$$
$$a_{long} \in [-a_{max}, 0]\,. \tag{4.11e}$$

where $p = \begin{bmatrix} p_1 & p_2 & p_3 & p_4 \end{bmatrix}$.

4.3.3 Intersection between constrained zonotopes and linear zonotopes with one or more unbounded dimensions

In proposition 1 in [19], the authors propose three operations for constrained zonotopes, linear transformation, Minkowski sum and intersection. In the article, an intersection between two constrained zonotopes is proposed but in case of an intersection between a constrained zonotope $\mathcal{Z}_c$ and a linear zonotope $\mathcal{Z}$, the intersection becomes,

$$\mathcal{Z}_c \cap \mathcal{Z} = \left\{ \begin{bmatrix} \mathbf{G}_{\mathcal{Z}c} & 0 \end{bmatrix}, c_{\mathcal{Z}c}, \begin{bmatrix} \mathbf{A} & 0 \\ \mathbf{G}_{\mathcal{Z}c} & -\mathbf{G}_{\mathcal{Z}} \end{bmatrix}, \begin{bmatrix} b \\ c_{\mathcal{Z}} - c_{\mathcal{Z}c} \end{bmatrix} \right\}. \tag{4.12}$$

Note that all generators in $\mathcal{Z}$ are added to the $\mathbf{A}$ matrix of $\mathcal{Z}_c$, regardless of whether these generators act as active constraints or not. This means that the number of rows

in the $\mathbf{A}$ matrix increases from n_c to n_c+n and the number of columns from $n_{g,\mathcal{Z}c}+1$ to $n_{g,\mathcal{Z}c} + n_{g,\mathcal{Z}}$, where n is the number of dimensions, n_c number of constraints in the constrained zonotope and n_g the number of generators.

In order to keep the $\mathbf{A}$ matrix as small as possible, we propose a minimalistic intersection method that can be useful when only one or a few constraints are added to a constrained zonotope, for example when a constrained zonotope is intersected with a half-space, which requires only one constraint.

Let $\mathcal{Z}_c$ be a constrained zonotope as defined in (4.3) and $\mathcal{Z}$ be a zonotope for which some dimensions may be unbounded and therefore have generators of length $\to \infty$.

Let's identify the unbounded states,

$$\mu = \left\{ i \;\middle|\; \exists g_{i,j} \to \pm\infty;\; j \in \{1, \dots, n_g\} \right\}, \tag{4.13}$$

where $g_{i,j}$ is the element of row i and column j in the matrix $\mathbf{G}$ and $i \in \mu$ are the indices of the unbounded states. If these states are removed from the zonotope then some generators may be left with length zero and therefore with no purpose. Let's identify those generators,

$$\gamma = \left\{ j \;\middle|\; g_{i,j} = 0 \;\forall\; i \in \{1, \dots, n \setminus \mu\} \right\}, \tag{4.14}$$

where $j \in \gamma$ are the indices of the generators that are left with length zero after removing the states of indices in μ.

A minimalistic intersection can be defined as,

$$\mathcal{Z}_c \cap \mathcal{Z} = \left\{ \begin{bmatrix} \mathbf{G}_{\mathcal{Z}c} & 0 \end{bmatrix}, c_{\mathcal{Z}c}, \begin{bmatrix} \mathbf{A} & 0 \\ \mathbf{G}_{\mathcal{Z}c}^{[\mu]} & -\mathbf{G}_{\mathcal{Z}}^{[\mu]\langle\gamma\rangle} \end{bmatrix}, \begin{bmatrix} b \\ c_{\mathcal{Z}}^{[\mu]} - c_{\mathcal{Z}c}^{[\mu]} \end{bmatrix} \right\}, \tag{4.15}$$

where $[\mu]$ denotes exclusion of the rows of indices $i \in \mu$ and $\langle\gamma\rangle$ the exclusion of columns of indices $j \in \gamma$.

4.3.4 Splitting constrained zonotopes

Constrained zonotopes are not as developed for practical purposes as linear zonotopes as this set representation was developed very recently and not all operations have been developed.

One important operation for reachability analysis of non-linearities systems is splitting reachable sets into two sets. The splitting operation of linear zonotopes can generally only be overapproximated although in some special cases an exact solution can be obtained. However, for constrained zonotopes, the splitting operation does not exists to the best of our knowledge. We therefore propose an exact general method to split a constrained zonotope $\mathcal{Z}_c$ along a dimension i, in two constrained

zonotopes $\mathcal{Z}_a$ and $\mathcal{Z}_b$,

$$\mathcal{Z}_a = \mathcal{Z} \cap \left\{ c + \begin{bmatrix} 0 \\ \vdots \\ 0 \\ \frac{\sup x_i - c_i}{2} \\ 0 \\ \vdots \\ 0 \end{bmatrix}, \begin{bmatrix} \infty & & & & & & \\ & \ddots & & & & & \\ & & \infty & & & & \\ & & & \frac{\sup x_i - c_i}{2} & & & \\ & & & & \infty & & \\ & & & & & \ddots & \\ & & & & & & \infty \end{bmatrix} \right\} \tag{4.16a}$$

$$\mathcal{Z}_b = \mathcal{Z} \cap \left\{ c - \begin{bmatrix} 0 \\ \vdots \\ 0 \\ \frac{\sup x_i - c_i}{2} \\ 0 \\ \vdots \\ 0 \end{bmatrix}, \begin{bmatrix} \infty & & & & & & \\ & \ddots & & & & & \\ & & \infty & & & & \\ & & & \frac{\sup x_i - c_i}{2} & & & \\ & & & & \infty & & \\ & & & & & \ddots & \\ & & & & & & \infty \end{bmatrix} \right\} \tag{4.16b}$$

where $\sup x_i$ is the supremum of the state x_i.

Note that the splitting operation proposed in (4.16) requires the minimalistic intersection method proposed in (4.15). In order to perform this operation with the intersection method in (4.12) one would have to replace the infinitely long generators with generators of finite length but long enough to enclose $\mathcal{Z}$ across all dimensions except i.

4.3.5 Graphical representation of constrained zonotopes

In order to plot a reachable set on a 2D canvas in an environment such as Matlab, the vertices of the set must be identified and line segments drawn between them. With V-represented polytopes, this is very straightforward since the vertices are already known. The vertices of H-represented polytopes and a linear zonotopes can also be identified relatively easily using so called *vertex enumeration*, a technique that includes solving a linear program. However, with constrained zonotopes, this problem is much more complicated and can quickly become unfeasible with a growing number of generators and constraints.

Based on the proposed method in (4.16), we propose a significantly more efficient way to approximate vertices of constrained zonotopes.

This method is the result of an idea discussed with Niklas Kochdumper (a PhD student under Prof. Dr.-Ing. Matthias Althoff at the Technical University of Munich, and one of the developers of the CORA toolbox), who suggested that we could, based

(a) Step 1. The constrained zonotope is projected along the two dimensions we want to plot.

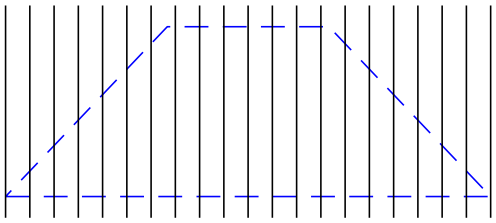

(b) Step 2. The constrained zonotope is sliced vertically in n even slices where n is the resolution of the approximation.

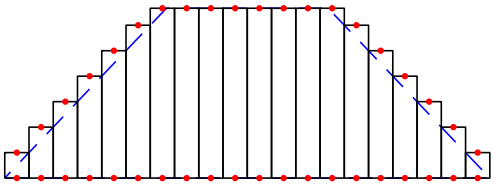

(c) Step 3. The intersection between the constrained zonotope and each slice is taken and over-approximated as parallelotopes. The center points of the top and the bottom sides of the parallelotopes are identified.

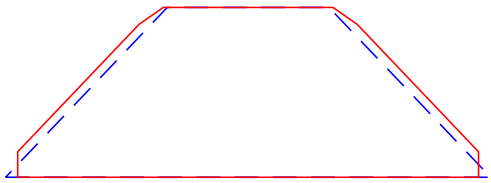

(d) Step 4. The approximated zonotope is the convex hull of the set of center points obtained in step 3.

Figure 4.5: An illustration of our proposed algorithm to plot constrained zonotopes.

on our proposed exact splitting method, recursively split the constrained zonotope into a set of constrained zonotopes, over-approximate each of them with intervals and then plot the intervals. Over-approximating constrained zonotopes with intervals, i.e. taking the interval-hull of a constrained zonotope, is not an expensive operation and can be done relatively fast.

The proposed method was implemented in Matlab as a function that takes a set of constrained zonotope along with the dimensions one wishes to plot and the resolution of the approximation. Plotting the convex hull of multiple sets is useful since CORA splits reachable sets of nonlinear systems in two sets when linearization tolerances are exceeded. The set of constrained zonotopes is sliced vertically in n even slices where n is the resolution of the approximation. The complexity of the algorithm grows linearily with increasing resolution.

In Figure 4.5, the core steps of the algorithm is illustrated were one constrained zonotope is approximated with a resolution of 20 slices.

To illustrate the efficiency of the proposed algorithm, the convex hull of 13 constrained zonotopes, each with 715-775 generators and 114-174 lines of constraints, took less than 66 s to plot on an laptop with a Intel Core i7-6600U CPU @ 2.60 GHz 2.81 GHz processor and 8 GB of RAM. For reference, constrained zonotopes of a sizes anywhere close to that would not be feasible to plot by vertex enumeration.

4.3.6 Implementation

The practical implementation for calculating reachable sets are discussed in this section. Initially, the reachable sets were calculated for the entire range of inputs, i.e., maximum to zero braking in combination with steering in both sides. It was observed that, for a reasonable bound on the linearization error, the calculation of sets became unfeasible as the number of splits grew exponentially. After examining the calculation of reachable sets for different input configurations, it was decided to calculate sets using two configurations, namely : i) for braking power ranging from 50 % to 100 % combined with steering in one side and ii) steering only to one side. The final sets were obtained by taking a convex hull of the two sets at every time step, with the assumption that the sets will always be convex for this analysis. Note that by splitting the input range it cannot be guaranteed that all the possible combinations of inputs are covered in the calculated sets. However, it can be guaranteed that the sets are conservative and the vehicle could perform better. The same methodology was repeated for the other direction for different constraints, as the vehicle is bounded by different constraints on the two sides. Moreover the delays accounted in the model for the two inputs, were not considered for reachability analysis and the vehicle's initial set is considered as a point located on the front of the vehicle.

Constrained zonotope was used to calculate constrained reachable sets in this thesis. The constraints were represented in the form of a zonotope, which was intersected with the calculated the set at every time-step. As mentioned earlier, intersecting the reachable sets with constraints at every time-step increases the number of constraints in the set, which naturally increases the computation complexity. To make the computations efficient for calculating reachable sets, the sets were reduced at every time-step using the inbuilt reduction feature of the toolbox. One of the most important parameters, which effects the computation complexity of the calculations of reachable sets, is the bound on linearization errors for different states, which also determines the splitting of the sets. In this thesis, the error bounds have be defined on state χ as :

$$e\chi = \begin{bmatrix} 0.2\,\mathrm{m} \\ 0.2\,\mathrm{m} \\ 3^{\circ} \\ 0.1\,\mathrm{m\,s^{-1}} \\ 0.1\,\mathrm{m\,s^{-2}} \\ 0.1\,\mathrm{m\,s^{-3}} \end{bmatrix}$$

where $e\chi$ is the error bound on the state $\chi = \begin{bmatrix} p_x & p_y & \phi & v & a_{lat} & j_{lat} \end{bmatrix}^T$. The reader can find other important parameters in B in Table B.1 and we strongly recommend them to follow the manual of the toolbox for extra details, see [1].

4.4 Reachability analysis results

In this section we present the results obtained from the reachability analysis using the model described in equation (4.10) without accounting for delays in different input signals, as mentioned earlier. All the reachability analysis implementations were done on a server having 6, 2.25 GHz Intel Xeon processors, and 64 GB memory.

Figure 4.6 illustrates the RSE trajectories and the reachable sets calculated using the model (4.10) for velocities $70\,\mathrm{km\,h^{-1}}$, $90\,\mathrm{km\,h^{-1}}$ and $120\,\mathrm{km\,h^{-1}}$.

The sets are calculated with the assumption that the car is on the right lane, so the constraints are different on the two sides of the vehicle to cope with the road layout. It can be observed when comparing the braking only trajectory of RSE and the reachable sets, that the vehicle covers a larger distance longitudinally. There could be two possible explanations for this characteristic: i) delays were considered while calculating RSE trajectories, while they were not considered while calculating

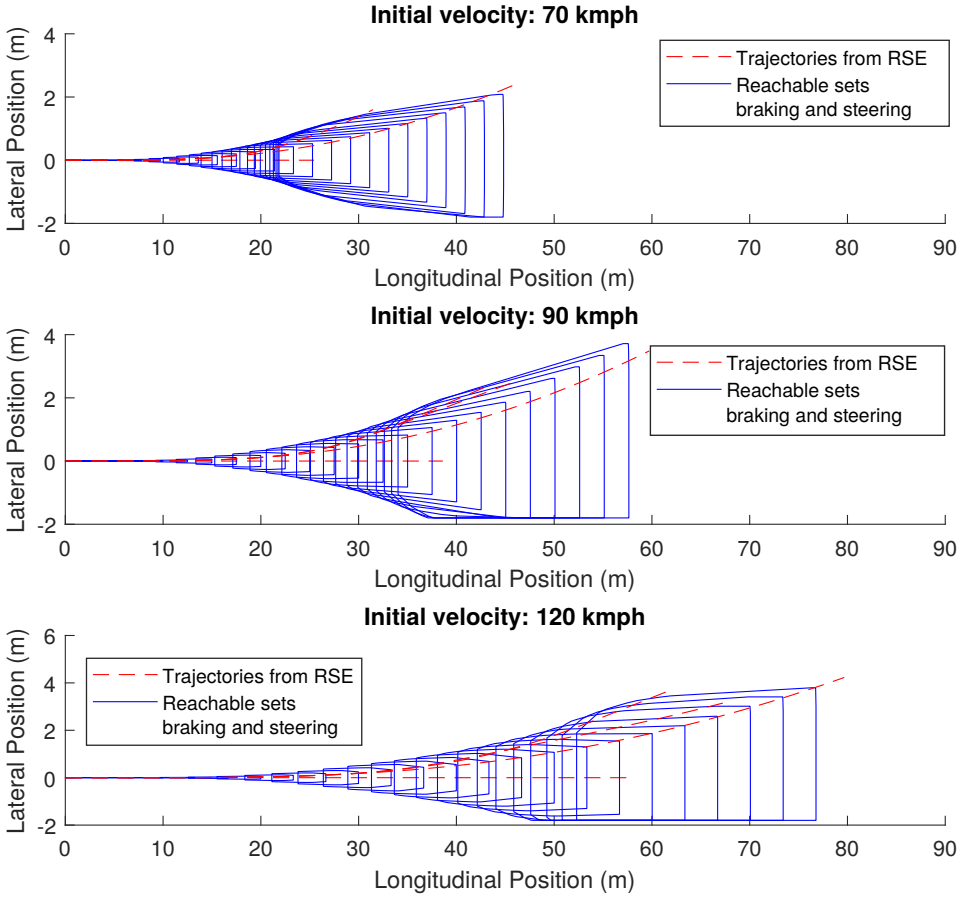

Figure 4.6: Reachable sets of the system for three different initial velocities, $70\,\mathrm{km\,h^{-1}}$, $90\,\mathrm{km\,h^{-1}}$ and $120\,\mathrm{km\,h^{-1}}$ evaluated for a time horizon between 0 and 2.4 s. The red dashed lines are trajectories obtained from RSE with different combinations of steering and braking.

reachable sets. ii) over-approximations in calculating sets due to the toolbox inbuilt features. Similar trend can be noticed when comparing the reachable sets with RSE trajectories, with steering only maneuvers. In addition to that, it is evident from the Figure 4.6 that the combination of different deceleration and steering inputs can help maneuvering the car to a higher lateral position faster, which can lead to great collision avoidance capabilities.

Figure 4.7 illustrates region reached by the vehicle using different control strategy for a specified time horizon. Green circles represent the positions acquired by the vehicle for maximum and no braking. These positions were calculated using Newton's equation for different braking powers. In addition to that sets in red and blue represent the reachables sets obtained for only steering- and combined braking and steering maneuvers. These sets were calculated using CORA toolbox. Sets obtained for combined braking and steering maneuvers includes the steering only sets. It is noticeable from Figure 4.7 that the vehicle can reach higher lateral positions quickly using combined braking and steering maneuvers when compared to steering only

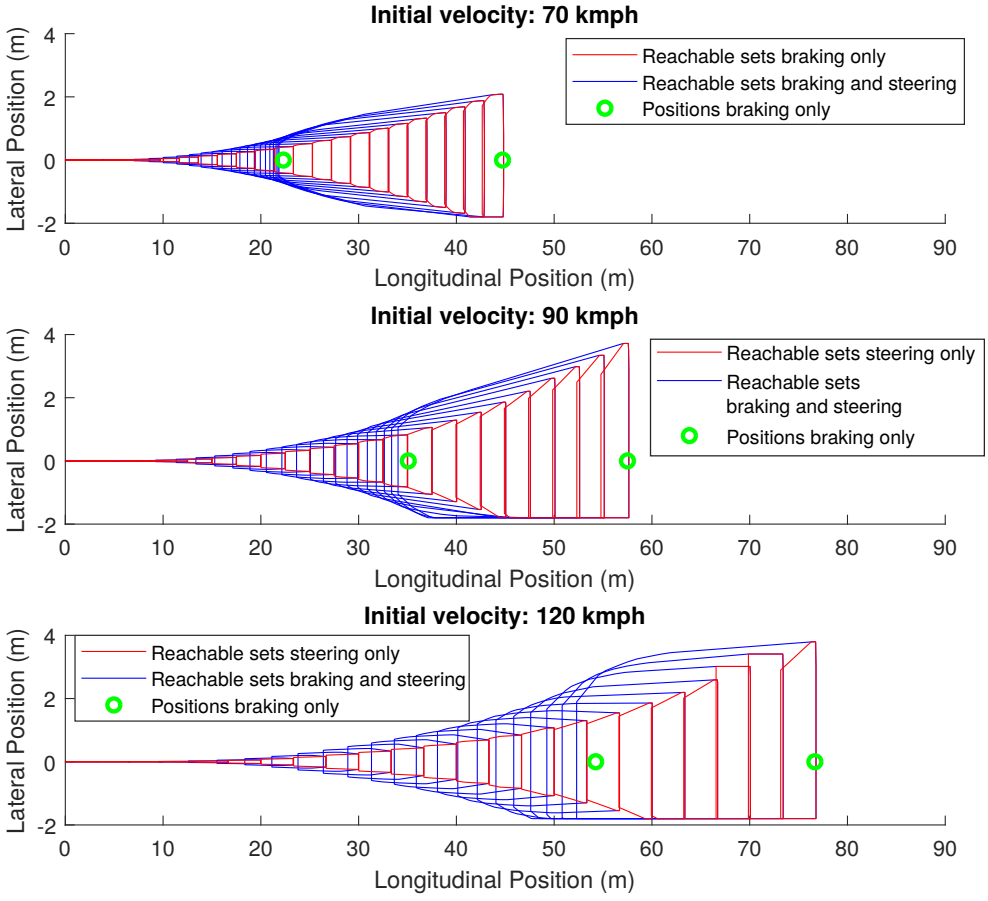

Figure 4.7: Reachable sets of the system for three different initial velocities, 70 km h^{-1}, 90 km h^{-1} and 120 km h^{-1} evaluated for a time horizon between 0 and 2.4 s. The sets represented in colours red and blue correspond to reachable sets using steering only and combined braking and steering maneuvers respectively. Green circles represent positions of the vehicle for maximum- and no braking.

Initial Velocity	**Time Horizon**	**Computation time**	
		Steering	Braking
50	2.0	42	982
70	2.8	6151	3.2×10^5
90	2.5	842	1.2×10^5
120	2.4	327	3.9×10^5
140	2.2	435	1.5×10^5
$(\mathrm{km\,h^{-1}})$	(s)	(s)	(s)

Table 4.1: Reachable sets computation time for different initial velocities.

maneuver, which could be beneficial for avoiding an collision laterally.

Table 4.1 represents the computation time for calculating reachable sets for different initial velocities. It is obvious that these calculations are quite resource intensive. In addition to that, one should not forget that this table just represents the time to calculate reachable sets for a given time horizon and does not consider the plotting operation of the sets, which is also computationally expensive.

5

Conclusions and perspectives

The main objective of this thesis was to establish and analyze the potential benefits of a combined braking- and steering maneuver with respect to braking only or steering only maneuvers. To perform this analysis, two methods were adopted: i) simulation based analysis using a Reference Simulation Environment (RSE) and ii) reachability analysis using the CORA toolbox for MATLAB.

5.1 Conclusions

Primarily, two conventional vehicle models, the kinematic bicycle model and the dynamic bicycle model, were compared to the vehicle modelled in the reference simulation environment. These models failed to capture the dynamics of the vehicle for combined braking and steering accurately enough which resulted in the formulation of a new model presented in Chapter 2. Simulations with a reference simulation environment showed that new model represented the vehicle's dynamics much better when simultaneously applying braking and steering.

The simulation results presented in Chapter 3 indicate that collision avoidance system that leverage combined braking and steering maneuvers may be beneficial in certain traffic scenarios. In this thesis, we focused on four traffic scenarios, i) a scenario involving a stationary obstacle on the road, ii) pedestrian crossing the road, iii) oncoming vehicle on the opposite lane and iv) a vehicle cut-in scenario. Out of these scenarios, a combined braking and steering maneuver turned out to be particularly beneficial when driving at higher velocities in scenarios involving a stationary obstacle on the road and a pedestrian crossing the road. In these two scenarios, a combined braking and steering maneuver may allow less restrictive interventions that provide additional time to the driver to react, and in some cases avoid collisions that cannot be avoided with traditional collision avoidance systems. These two scenarios were also quite simple to abstract mathematically which enabled us to examine them quite thoroughly. For the two remaining scenarios, the oncoming scenario and the vehicle cut-in scenario, the simulation results did not reveal significant benefits as explicitly.

In addition to that, the performed reachability analysis indicated that a combined

braking and steering maneuver may allow the vehicle to reach configurations not accessible by independent braking or steering actuation-based systems. The obtained results are overapproximated as the longitudinal and lateral dynamics of a vehicle exposed to braking and steering simultaneously turned out to be too nonlinear and complex to obtain accurate results from with reachability analysis. The research did however result in new algorithms being developed that turned out to be very helpful when performing reachability analysis using zonotopes. These algorithms are: i) splitting constrained zonotopes, ii) efficiently intersecting constrained zonotopes with state constraints and iii) efficiently plotting constrained zonotopes with a high number of constraints.

5.2 Perspectives

From the two methods used to derive results in this thesis we obtained from the reachability analysis, over-approximated, general results and from the simulation analysis, conservative results targeted for specific use cases. In order to attempt to obtain more accurate general results we would like to suggest the following to be considered:

- In an email conversation with the authors of the CORA toolbox, they mentioned that they were working on an implementation of constrained polynomial zonotopes as well as general polynomial zonotopes of any order. It would be very interesting to see how closely the system considered in this thesis could be approximated with a constrained higher order polynomial zonotope and how accurate the results yielded from such representation could be.

- In [3], M. Althoff discusses several techniques used for reachability analysis of non-linear systems, one of which is based on the idea of reformulating the problem into an optimization problem. It would be very interesting to investigate how such methods would perform in relation to our problem.

In addition to these suggestions we would like to propose a further investigation on the vehicle cut-in scenario with a simulation based approach. As stated before, we found in our research that a combined braking a steering maneuver turned out to be particularly beneficial in two scenarios, a stationary obstacle on the road where the longitudinal velocity of the host vehicle was high, and secondly in scenarios involving a pedestrian crossing the road where the threat has a non-zero lateral velocity. The cut-in scenario can be viewed as a combination of these two scenarios since the host has a non-zero longitudinal velocity and the threat has both a longitudinal- and a lateral velocity. This makes the vehicle-cut in scenario very promising for further research.

Bibliography

[1] M. Althoff. "An Introduction to CORA 2015". In: *Proc. of the Workshop on Applied Verification for Continuous and Hybrid Systems*. 2015.

[2] M. Althoff. "Reachability Analysis and its Application to the Safety Assessment of Autonomous Cars". http://nbn-resolving.de/urn/resolver.pl?urn:nbn:de:bvb:91-diss-20100715-963752-1-4. Dissertation. Technische Universität München, 2010.

[3] M. Althoff. "Reachability Analysis of Nonlinear Systems using Conservative Polynomialization and Non-Convex Sets". In: *Hybrid Systems: Computation and Control*. 2013, pp. 173–182.

[4] M. Althoff and B. H. Krogh. "Zonotope Bundles for the Efficient Computation of Reachable Sets". In: *Proc. of the 50th IEEE Conference on Decision and Control*. 2011, pp. 6814–6821.

[5] M. Brannstrom, E. Coelingh, and J. Sjoberg. "Model-Based Threat Assessment for Avoiding Arbitrary Vehicle Collisions". In: *IEEE Transactions on Intelligent Transportation Systems* 11.3 (Sept. 2010), pp. 658–669.

[6] Volvo Cars. *Collision Avoidance Concept*. [Online]. 2009. URL: `https://www.media.volvocars.com/global/en-gb/media/photos/list`.

[7] J. Dahl, G. Rodrigues de Campos, C. Olsson, and J. Fredriksson. "Collision Avoidance: a Literature Review on Threat-Assessment Techniques". In: *IEEE Transactions on Intelligent Transportation Systems* (2018- To appear).

[8] A. Eckert, B. J. Hartmann, M. Sevenich, and Dr. P. E. Rieth. "Emergency Steer Brake Assist – a Systematic Approach for System Integration of Two Complementary Driver Assistance Systems". In: 2011.

[9] K. Eriksson, D. Estep, and C. Johnson. "Lipschitz Continuity". In: *Applied Mathematics: Body and Soul: Volume 1: Derivatives and Geometry in IR3*. Berlin, Heidelberg: Springer Berlin Heidelberg, 2004, pp. 149–164. URL: `https://doi.org/10.1007/978-3-662-05796-4_12`.

[10] P. Falcone, M. Ali, and J. Sjoberg. "Predictive Threat Assessment via Reachability Analysis and Set Invariance Theory". In: *IEEE Transactions on Intelligent Transportation Systems* 12.4 (Dec. 2011), pp. 1352–1361.

[11] R. L. French, Y. Noguchi, and K. Sakamoto. "International competitiveness in IVHS: Europe, Japan, and the United States". In: *Proceedings of VNIS'94 - 1994 Vehicle Navigation and Information Systems Conference*. Aug. 1994, pp. 525–530.

[12] M. Herceg, M. Kvasnica, C.N. Jones, and M. Morari. "Multi-Parametric Toolbox 3.0". In: *Proc. of the European Control Conference*. `http://control.ee.ethz.ch/~mpt`. Zürich, Switzerland, July 2013, pp. 502–510.

[13] M. Koschi and M. Althoff. “SPOT: A tool for set-based prediction of traffic participants”. In: *2017 IEEE Intelligent Vehicles Symposium (IV)*. June 2017, pp. 1686–1693.

[14] Mark Mikofski. *polyVal2D and polyFit2D*. Version 1.1.0.0. Apr. 18, 2013. URL: https://se.mathworks.com/matlabcentral/fileexchange/41097-polyval2d-and-polyfit2d.

[15] World Health Organization. *Global status report on road safety 2018*. URL: https://www.who.int/violence_injury_prevention/road_safety_status/2018/en/.

[16] B. Paden et al. “A Survey of Motion Planning and Control Techniques for Self-Driving Urban Vehicles”. In: *IEEE Transactions on Intelligent Vehicles* 1.1 (Mar. 2016), pp. 33–55.

[17] R. Rajamani. *Vehicle dynamics and control*. Springer, 2011.

[18] Thatcham Research. *Autonomous Emergency Braking (AEB) - Frequently Asked Questions*. URL: https://www.thatcham.org/files/pdf/AEB_FAQ.pdf.

[19] J. K. Scott, D. M. Raimondo, G. R. Marseglia, and R. D. Braatz. “Constrained zonotopes: A new tool for set-based estimation and fault detection”. In: *Automatica* 69 (2016), pp. 126–136.

[20] T. Shim, G. Adireddy, and H. Yuan. “Autonomous vehicle collision avoidance system using path planning and model-predictive-control-based active front steering and wheel torque control”. In: *Proceedings of the Institution of Mechanical Engineers, Part D: Journal of Automobile Engineering* 226.6 (2012), pp. 767–778. URL: https://doi.org/10.1177/0954407011430275.

[21] S. Söntges, M. Koschi, and M. Althoff. “Worst-case Analysis of the Time-To-React Using Reachable Sets”. In: *Proc. of the IEEE Intelligent Vehicles Symposium*. 2018, pp. 1891–1897.

[22] Statista. *Number of road traffic fatalities in Sweden from 2006 to 2015*. URL: https://www.statista.com/statistics/438009/number-of-road-deaths-in-sweden/.

[23] Association for safe international road travel. *Annual Global Road Crash Statistics*. URL: http://asirt.org/initiatives/informing-road-users/road-safety-facts/road-crash-statistics.

Appendices

A

RSE Simulation Results

A.1 Traffic scenarios involving a stationary obstacle on the road

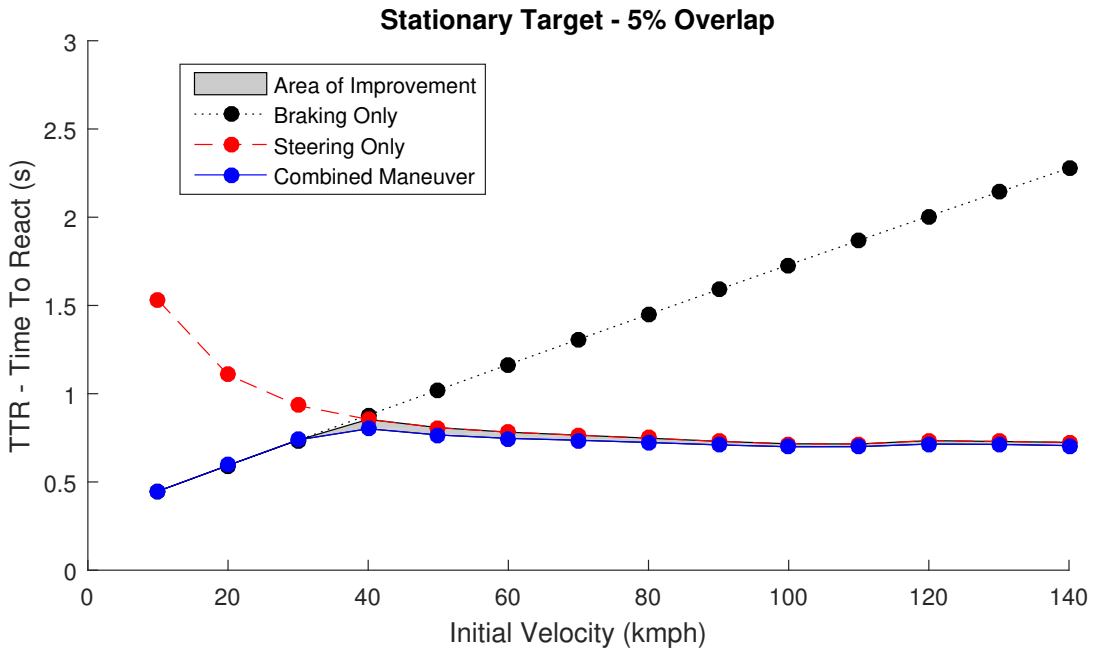

Figure A.1: Combined braking and steering maneuver compared to braking only and steering only maneuvers when approaching a stationary obstacle on the road with a 5 % overlap.

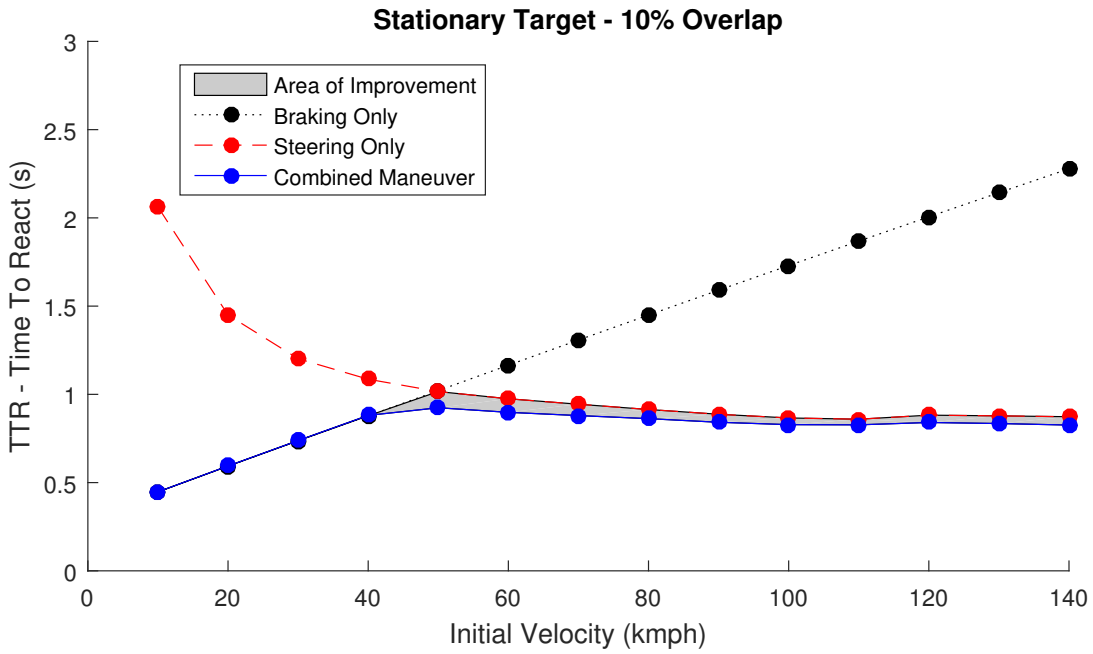

Figure A.2: Combined braking and steering maneuver compared to braking only and steering only maneuvers when approaching a stationary obstacle on the road with a 10 % overlap.

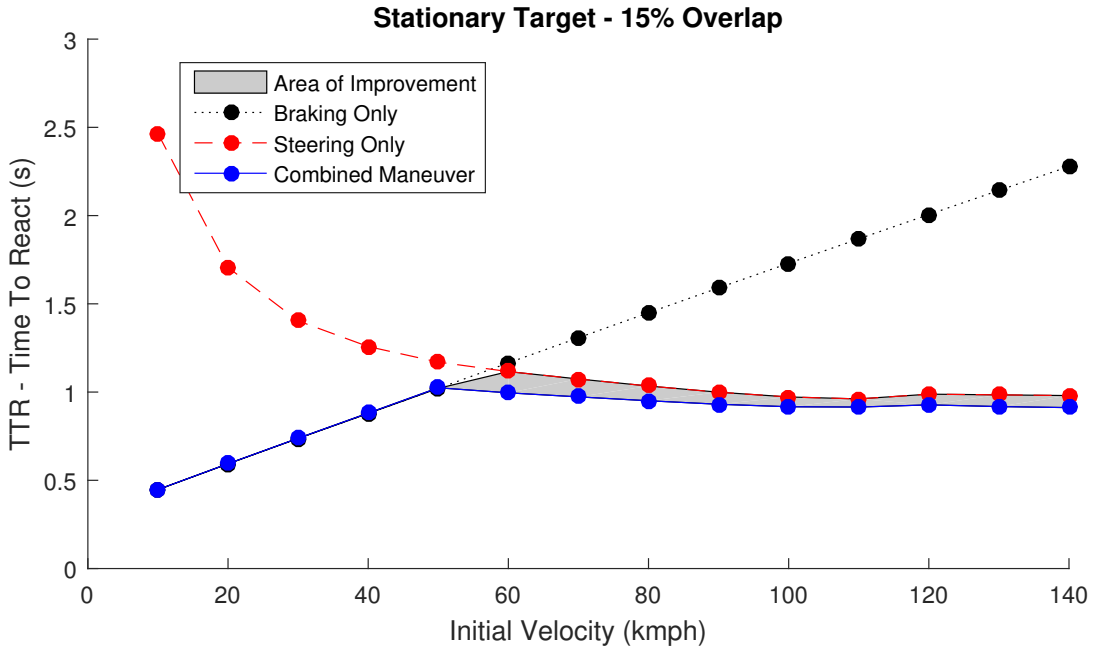

Figure A.3: Combined braking and steering maneuver compared to braking only and steering only maneuvers when approaching a stationary obstacle on the road with a 15 % overlap.

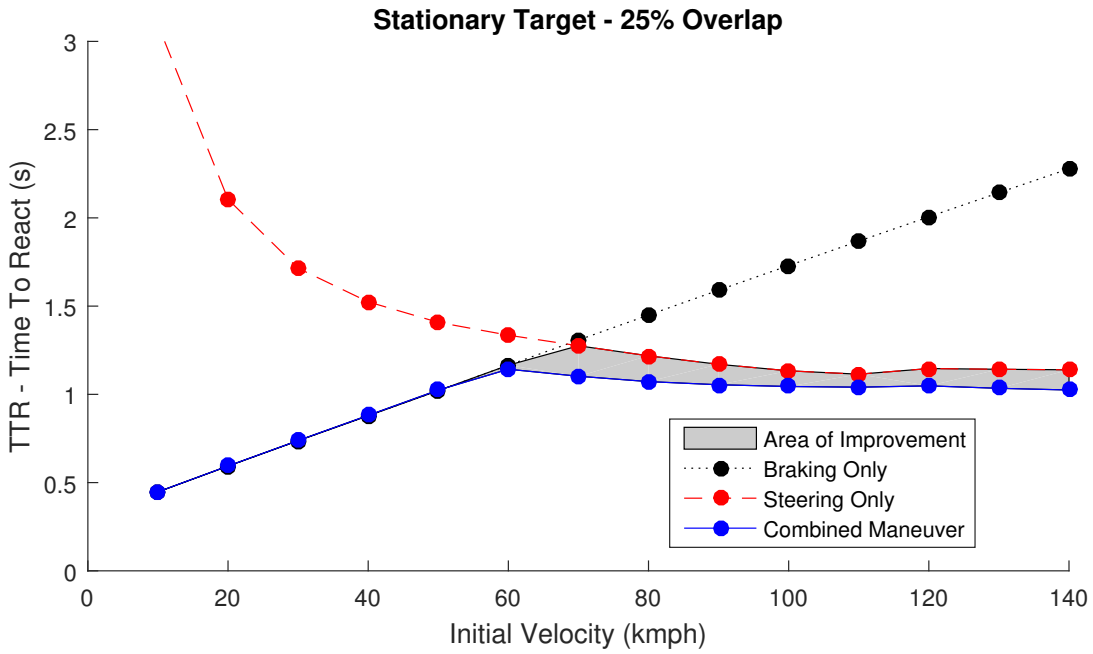

Figure A.4: Combined braking and steering maneuver compared to braking only and steering only maneuvers when approaching a stationary obstacle on the road with a 25 % overlap.

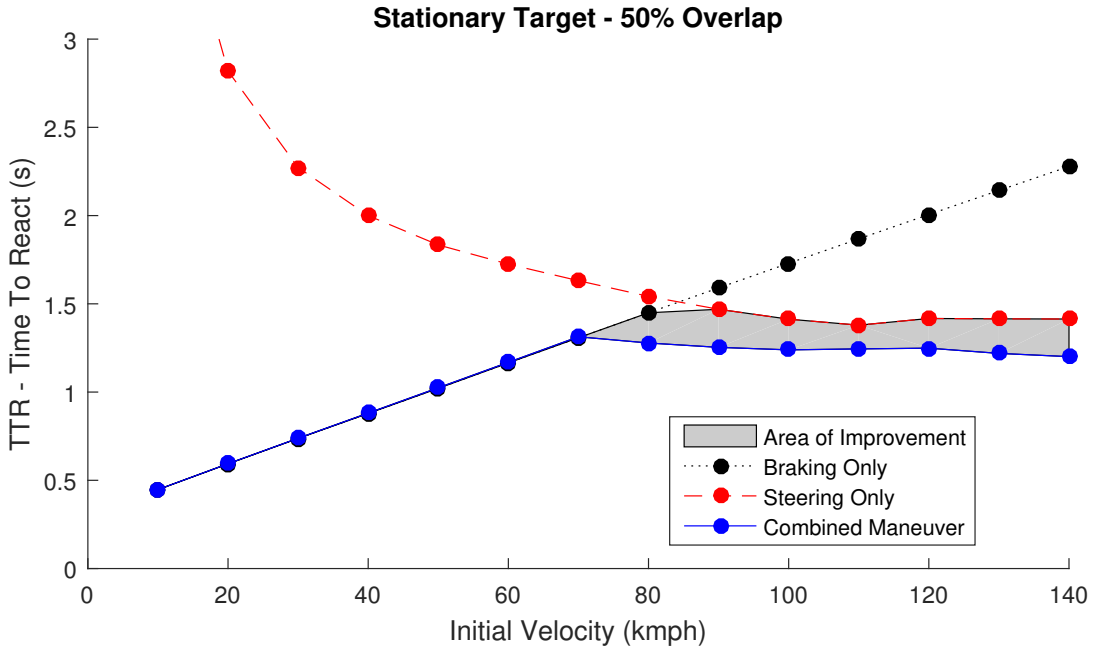

Figure A.5: Combined braking and steering maneuver compared to braking only and steering only maneuvers when approaching a stationary obstacle on the road with a 50 % overlap.

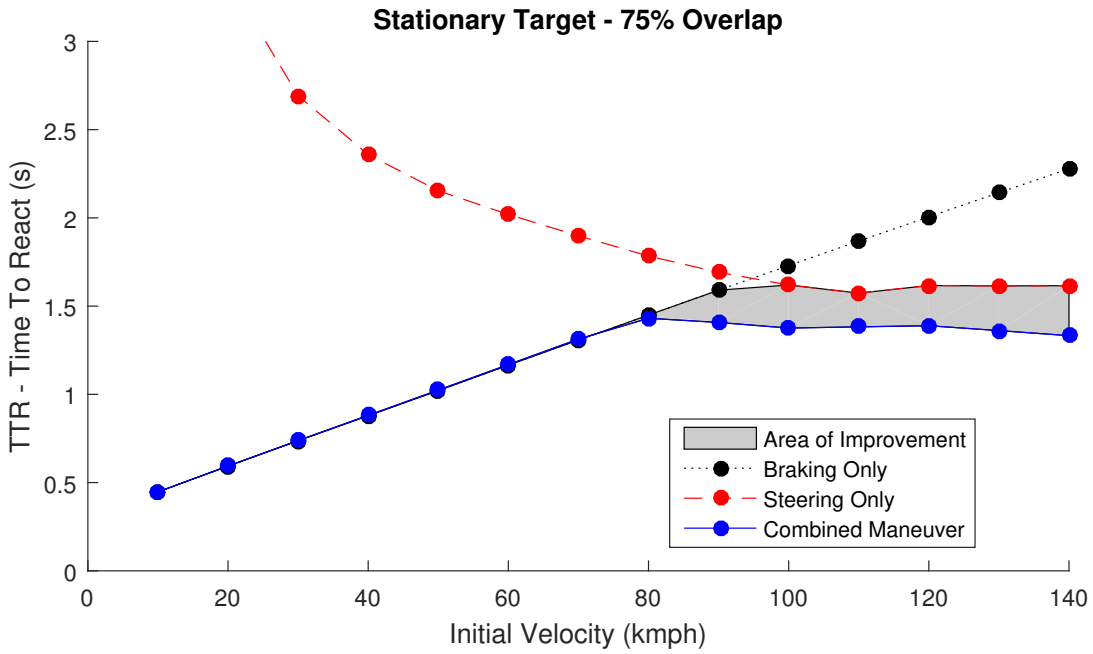

Figure A.6: Combined braking and steering maneuver compared to braking only and steering only maneuvers when approaching a stationary obstacle on the road with a 75 % overlap.

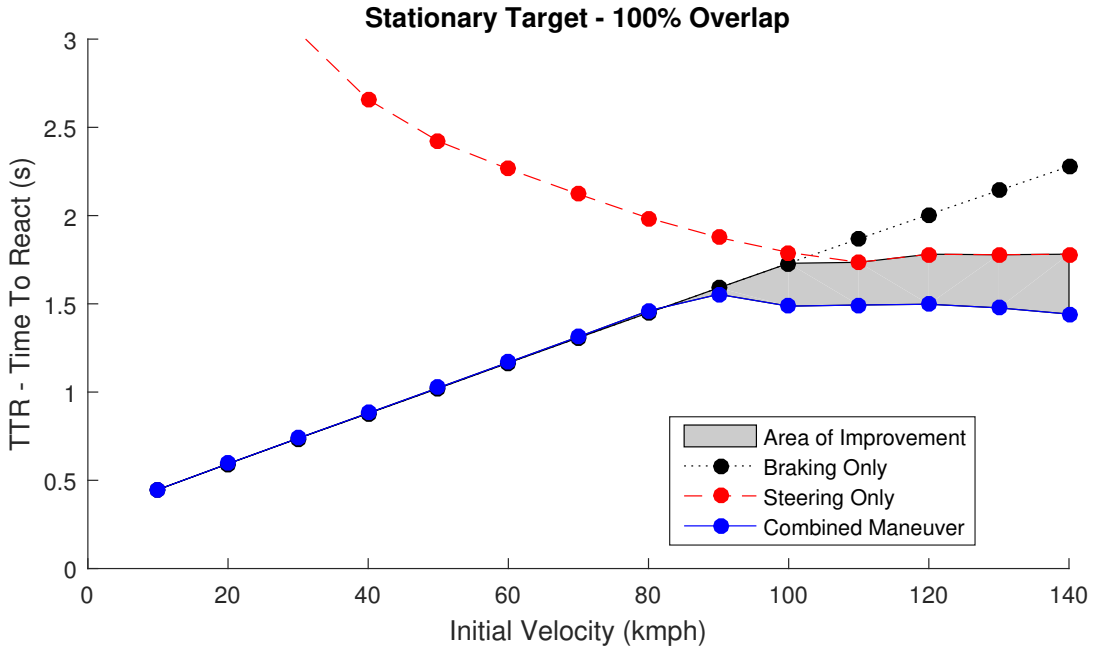

Figure A.7: Combined braking and steering maneuver compared to braking only and steering only maneuvers when approaching a stationary obstacle on the road with a 100 % overlap.

A.2 Traffic scenarios involving an oncoming vehicle from the opposite lane

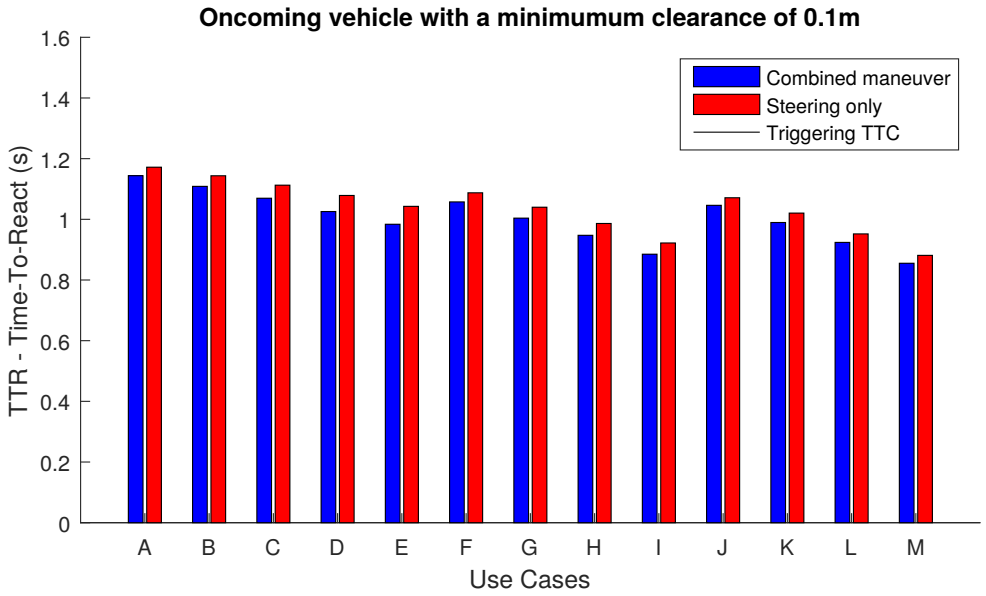

Figure A.8: Combined braking and steering maneuver compared to a steering only maneuver when approaching an oncoming vehicle from the opposite lane, accounting for 10 cm clearance.

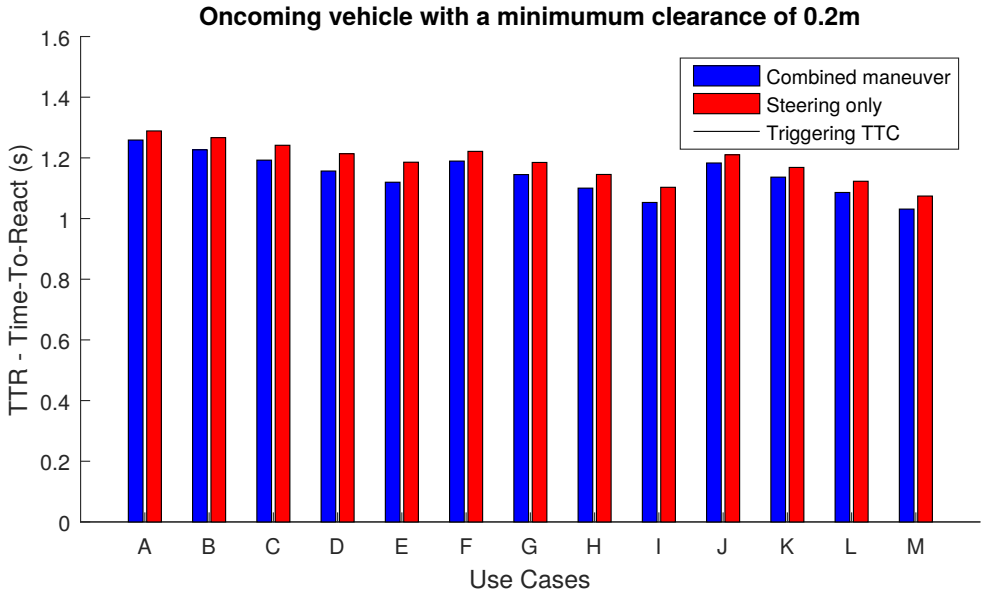

Figure A.9: Combined braking and steering maneuver compared to a steering only maneuver when approaching an oncoming vehicle from the opposite lane, accounting for 20 cm clearance.

A.3 Traffic scenarios involving a pedestrian crossing the road

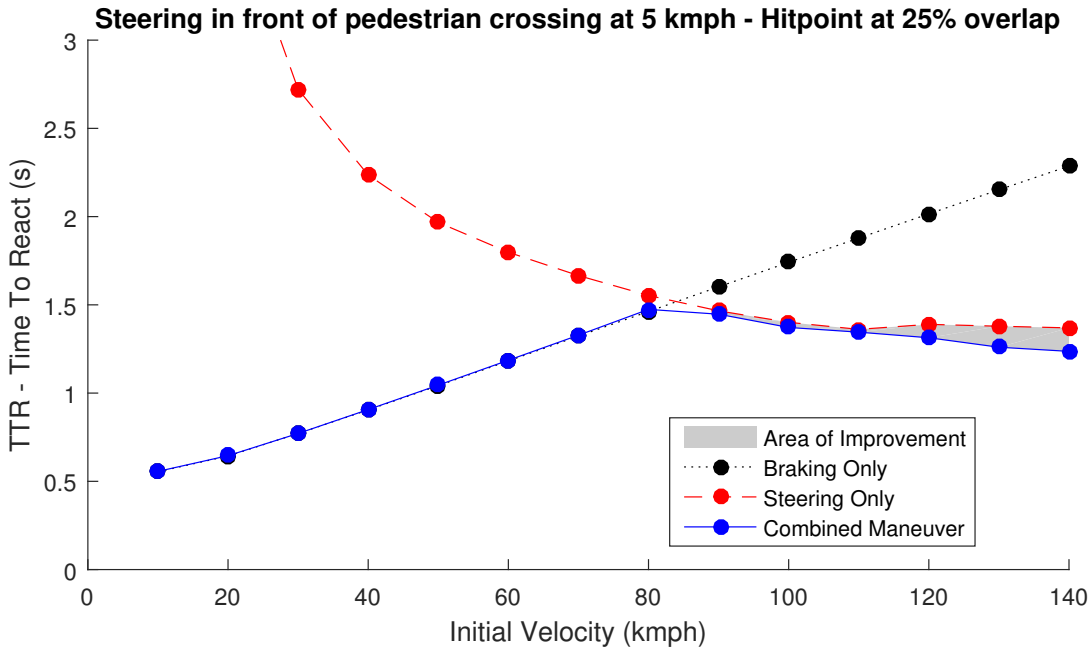

Figure A.10: Combined braking and steering maneuver compared to braking only and steering only maneuvers when attempting to steer in front of a pedestrian crossing the road at $5\,\mathrm{km\,h^{-1}}$, approaching a collision with a hitpoint at 25 % overlap.

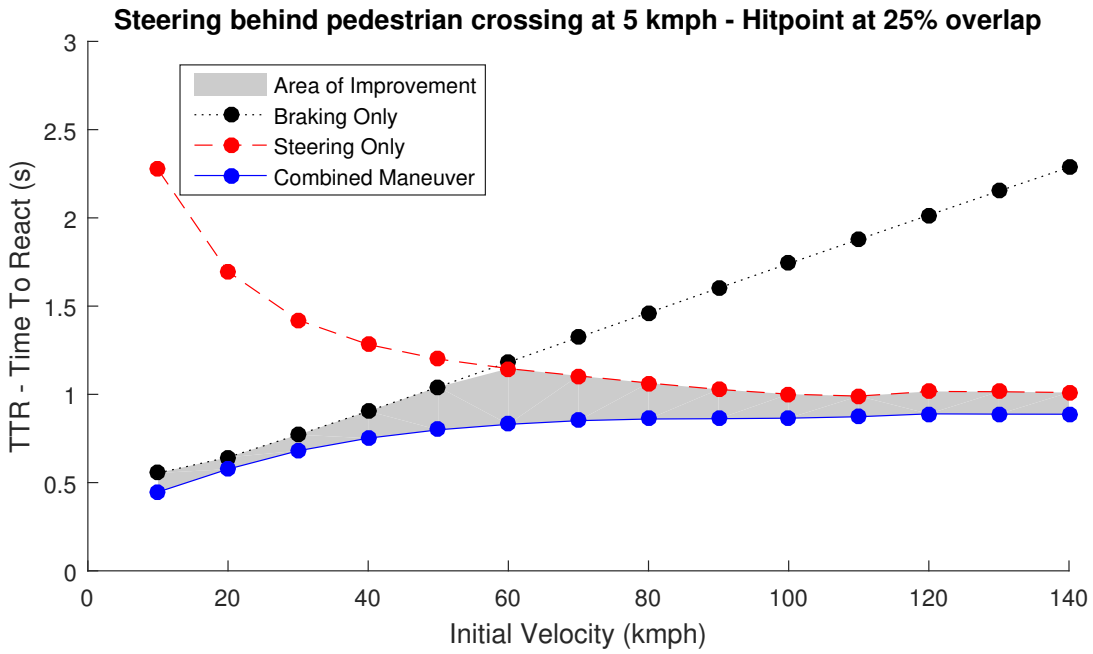

Figure A.11: Combined braking and steering maneuver compared to braking only and steering only maneuvers when attempting to steer behind a pedestrian crossing the road at $5\,\mathrm{km\,h^{-1}}$, approaching a collision with a hitpoint at 25 % overlap.

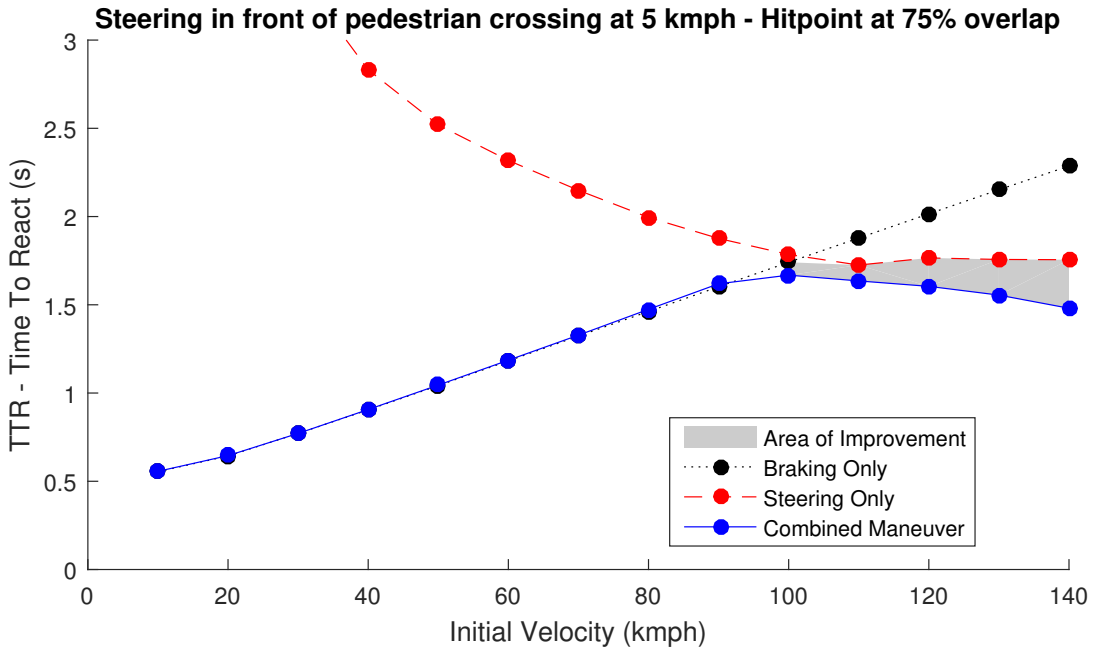

Figure A.12: Combined braking and steering maneuver compared to braking only and steering only maneuvers when attempting to steer in front of a pedestrian crossing the road at $5\,\mathrm{km\,h^{-1}}$, approaching a collision with a hitpoint at 75 % overlap.

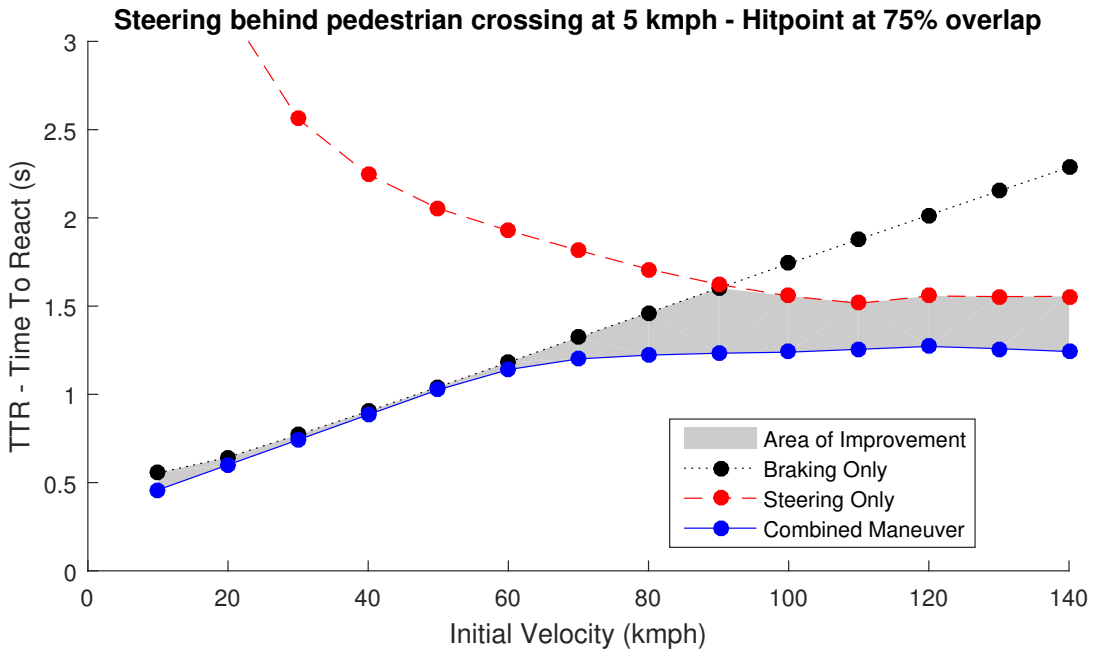

Figure A.13: Combined braking and steering maneuver compared to braking only and steering only maneuvers when attempting to steer behind a pedestrian crossing the road at $5\,\mathrm{km\,h^{-1}}$, approaching a collision with a hitpoint at 75 % overlap.

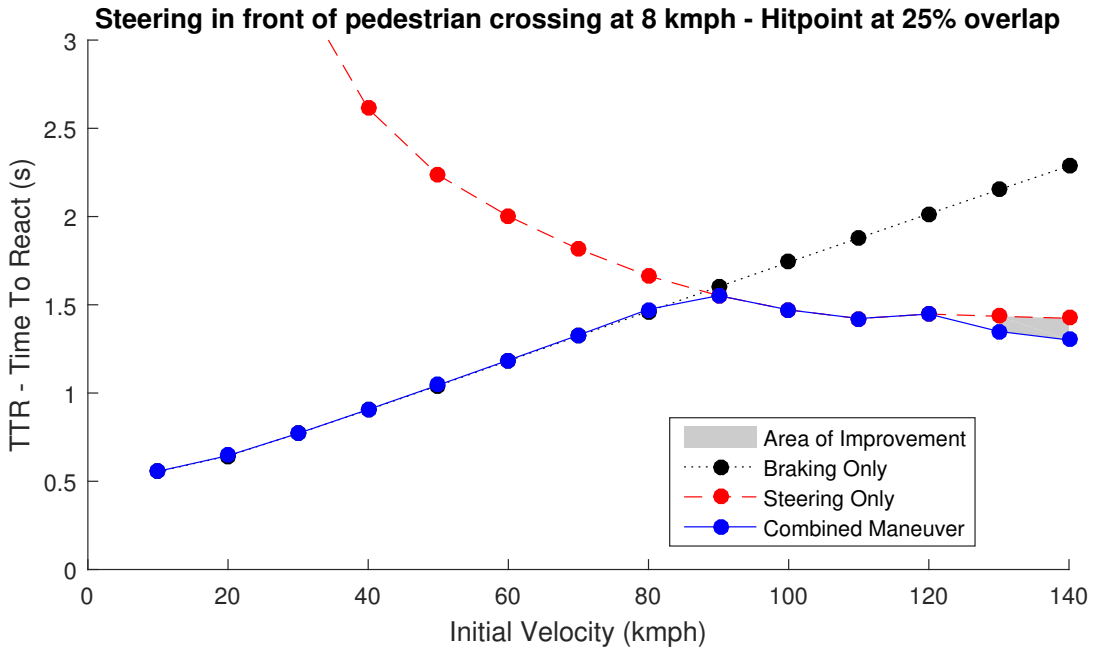

Figure A.14: Combined braking and steering maneuver compared to braking only and steering only maneuvers when attempting to steer in front of a pedestrian crossing the road at $8\,\mathrm{km\,h^{-1}}$, approaching a collision with a hitpoint at 25 % overlap.

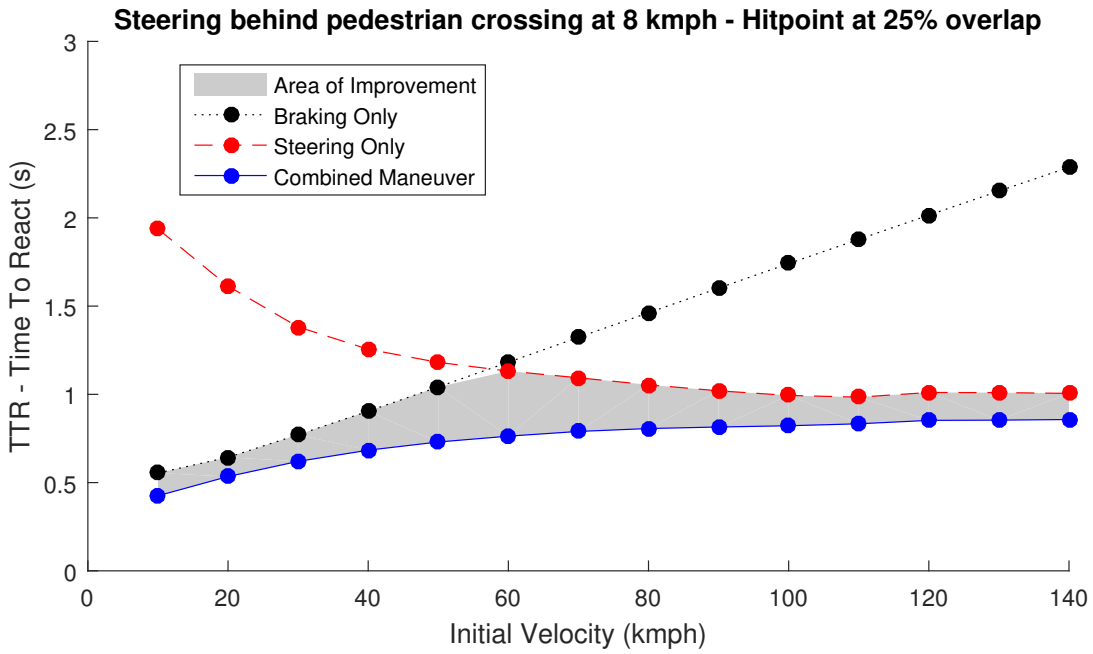

Figure A.15: Combined braking and steering maneuver compared to braking only and steering only maneuvers when attempting to steer behind a pedestrian crossing the road at $8\,\mathrm{km\,h^{-1}}$, approaching a collision with a hitpoint at 25 % overlap.

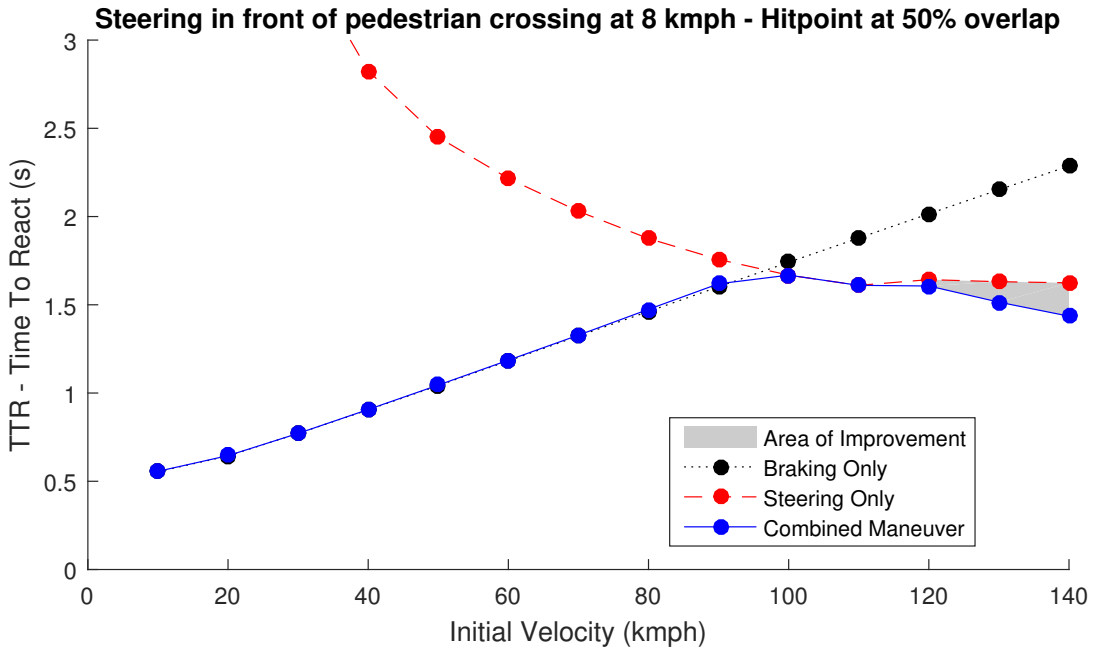

Figure A.16: Combined braking and steering maneuver compared to braking only and steering only maneuvers when attempting to steer in front of a pedestrian crossing the road at $8\,\mathrm{km\,h^{-1}}$, approaching a collision with a hitpoint at 50 % overlap.

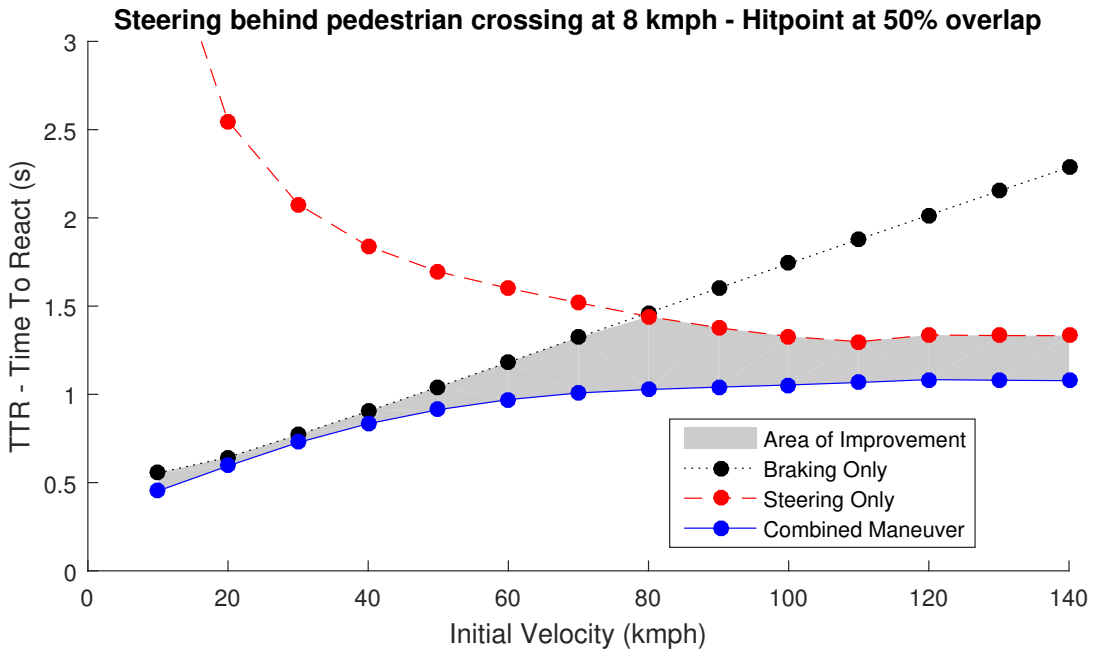

Figure A.17: Combined braking and steering maneuver compared to braking only and steering only maneuvers when attempting to steer behind a pedestrian crossing the road at $8\,\mathrm{km\,h^{-1}}$, approaching a collision with a hitpoint at 50 % overlap.

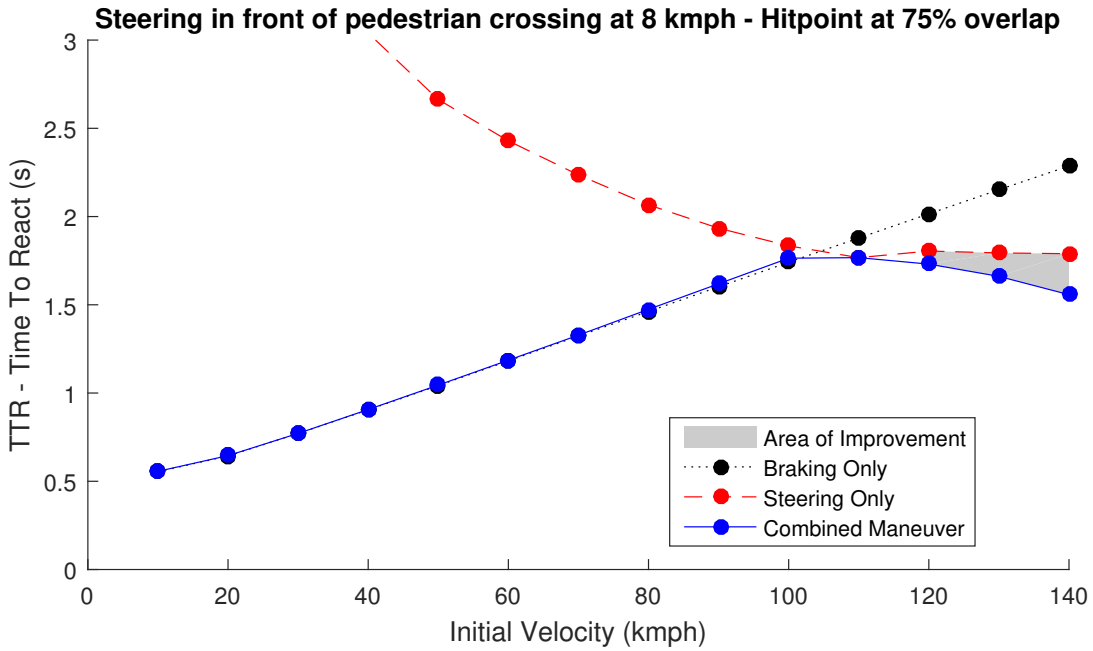

Figure A.18: Combined braking and steering maneuver compared to braking only and steering only maneuvers when attempting to steer in front of a pedestrian crossing the road at $8\,\mathrm{km\,h^{-1}}$, approaching a collision with a hitpoint at 75 % overlap.

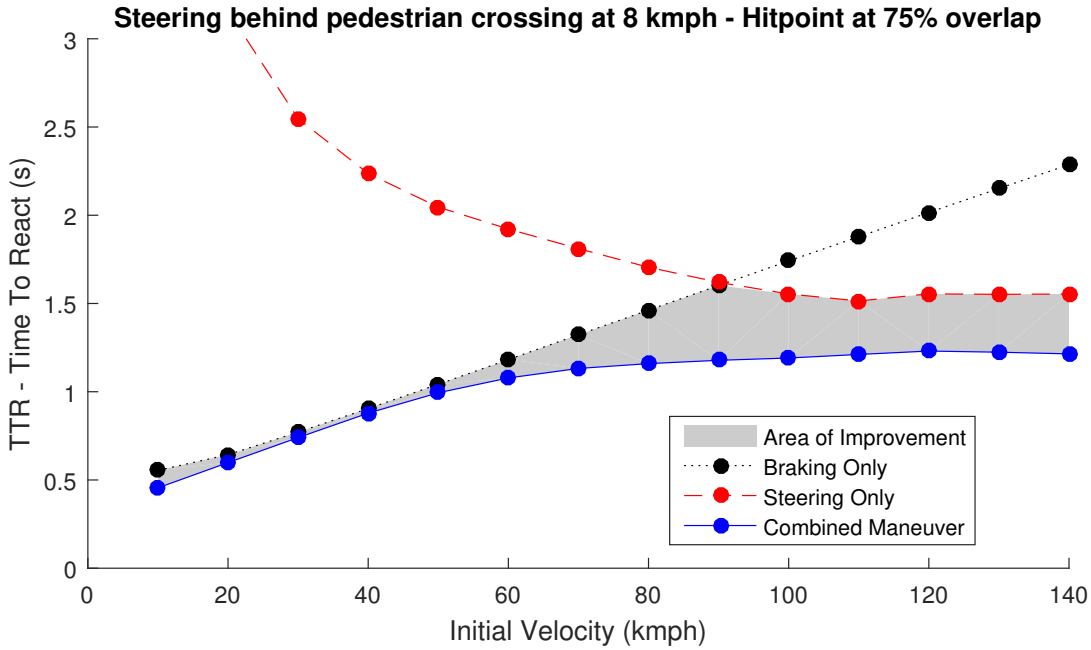

Figure A.19: Combined braking and steering maneuver compared to braking only and steering only maneuvers when attempting to steer behind a pedestrian crossing the road at $8\,\mathrm{km\,h^{-1}}$, approaching a collision with a hitpoint at 75 % overlap.

B

Reachability Analysis

Parameter	Value
`timeStep`	0.1
`errorOrder`	10
`taylorTerms`	4
`reductionInterval`	10^3
`maximumZonotopeOrder`	20
`polytopeOrder`	2
`intermediateOrder`	5
`advancedLinErrorComp`	0

Table B.1: Parameters used for reachability analysis.